

This is an Open Access document downloaded from ORCA, Cardiff University's institutional repository: <https://orca.cardiff.ac.uk/id/eprint/108126/>

This is the author's version of a work that was submitted to / accepted for publication.

Citation for final published version:

Kwelwa, S.D., Sanislav, I.V., Dirks, P.H.G.M., Blenkinsop, Thomas and Kolling, S.L. 2018. The petrogenesis of the Neoproterozoic Kukuluma Intrusive Complex, NW Tanzania. *Precambrian Research* 305 , pp. 64-78. 10.1016/j.precamres.2017.12.021

Publishers page: <http://dx.doi.org/10.1016/j.precamres.2017.12.021>

Please note:

Changes made as a result of publishing processes such as copy-editing, formatting and page numbers may not be reflected in this version. For the definitive version of this publication, please refer to the published source. You are advised to consult the publisher's version if you wish to cite this paper.

This version is being made available in accordance with publisher policies. See <http://orca.cf.ac.uk/policies.html> for usage policies. Copyright and moral rights for publications made available in ORCA are retained by the copyright holders.



## Accepted Manuscript

The petrogenesis of the Neoproterozoic Kukuluma Intrusive Complex, NW Tanzania

S.D. Kwelwa, I.V. Sanislav, P.H.G.M. Dirks, T. Blenkinsop, S.L. Kolling

PII: S0301-9268(17)30447-3

DOI: <https://doi.org/10.1016/j.precamres.2017.12.021>

Reference: PRECAM 4966

To appear in: *Precambrian Research*

Received Date: 1 August 2017

Revised Date: 4 October 2017

Accepted Date: 4 December 2017

Please cite this article as: S.D. Kwelwa, I.V. Sanislav, P.H.G.M. Dirks, T. Blenkinsop, S.L. Kolling, The petrogenesis of the Neoproterozoic Kukuluma Intrusive Complex, NW Tanzania, *Precambrian Research* (2017), doi: <https://doi.org/10.1016/j.precamres.2017.12.021>

This is a PDF file of an unedited manuscript that has been accepted for publication. As a service to our customers we are providing this early version of the manuscript. The manuscript will undergo copyediting, typesetting, and review of the resulting proof before it is published in its final form. Please note that during the production process errors may be discovered which could affect the content, and all legal disclaimers that apply to the journal pertain.





23 ( $\text{Na}_2\text{O}_{\text{average}} = 5.61 \text{ wt } \%$ ),  $\text{Dy}/\text{Yb}_n$  ( $\text{Dy}/\text{Yb}_{n\text{-average}} = 2.21$ ), a negative Sr anomaly and  
24 correlated Nb/La and Zr/Sm ratios consistent with derivation from partial melting of eclogite  
25 with residual rutile. Small variations in the Th/U ratio and near chondritic/MORB average  
26 values ( $\text{Th}/\text{U}_{\text{monzonite}} = 3.65$ ;  $\text{Th}/\text{U}_{\text{diorite}} = 2.92$ ) are inconsistent with a subducting slab  
27 signature, and it is proposed that the monzonite and the diorite suites of the KIC formed by  
28 partial melting of garnet-bearing, lower mafic crust of an oceanic plateau. The granodiorite  
29 suite has lower Mg# ( $\text{Mg}\#_{\text{average}} = 41$ ), moderately fractionated REE, low Sr/Y ( $\text{Sr}/\text{Y}_{\text{average}} =$   
30  $20$ ), La/Yb ( $\text{La}/\text{Yb}_{\text{average}} = 15$ ),  $\text{Dy}/\text{Yb}_n$  ( $\text{Dy}/\text{Yb}_{n\text{-average}} = 1.24$ ) and small negative Eu anomalies  
31 suggesting derivation from partial melting of amphibolite and plagioclase fractionation. Near-  
32 MORB Th/U ( $\text{Th}/\text{U}_{\text{average}} = 2.92$ ) and Zr/Sm ( $\text{Zr}/\text{Sm}_{\text{average}} = 30.21$ ) ratios are consistent with  
33 intracrustal melting of amphibolite.

34 Archean rocks with an “adakitic” geochemical signature have been used to argue in  
35 favour of a plate tectonics regime in the Archean. The results presented here suggest that  
36 tectonic models for the Tanzania Craton, which invoke a subduction-related setting for all  
37 greenstone belts may need revision.

38

## 39 **Introduction**

40 The geochemical signature of intermediate to felsic rocks with fractionated REE  
41 patterns and high Sr/Y and La/Yb ratios has been interpreted to indicate melt derivation from  
42 a subducted slab at amphibolite to eclogite facies conditions (Defant and Drummond, 1990;  
43 Drummond and Defant, 1990). Their particular geochemical signature, including a high Mg#  
44 (molecular ( $\text{Mg}/\text{Mg}+\text{Fe}$ )  $\times 100$ ) and enriched large-ion lithophile elements (LILE) were  
45 interpreted to represent different degrees of interaction between slab melts and mantle  
46 peridotite in the mantle wedge (e.g. Kay, 1978; Tatsumi and Ishizaka, 1981; Shirey and



47 Hanson, 1984; Stern et al., 1989; Defant and Drummond, 1990; Drummond and Defant,  
48 1990; Tatsumi, 2006; Moyen, 2009; Castillo, 2012). Arc rocks with similar geochemical  
49 signatures, including andesite, dacite, sodic rhyolite and their plutonic equivalents, were  
50 grouped under the term “adakites” by Defant and Drummond (1990) implying they share a  
51 specific petrogenetic history, namely, melting of the subducted slab. Another class of rocks  
52 sharing similar petrogenetic processes (e.g. melting of mantle peridotite metasomatised by  
53 subduction fluids/melts) and geochemically similar to adakites includes the high-Mg  
54 andesites or sanukitoids (e.g. Tatsumi and Ishizaka, 1981; Shirey and Hanson, 1984; Tatsumi,  
55 2006; Tatsumi, 2008), and the crustal contaminated sanukitoids of South India described as  
56 “Closepet-type” granites (Jayanada et al., 1995).

57 Both adakites and sanukitoids are derived from melting of a metamorphosed, garnet-  
58 bearing, mafic igneous rock protolith (e.g. Thorkelson and Breitsprecher, 2005). In the case  
59 of sanukitoids this probably involved melting of a metasomatised mantle wedge, and in the  
60 case of adakites the subducting slab, but the important message is that both suites are  
61 generally interpreted as imparting a subduction signature. Martin et al. (2005) subdivided  
62 adakites into two groups, low-silica adakites (LSA) and high-silica adakites (HSA),  
63 corresponding to distinct petrogenetic processes. In this subdivision the petrogenesis of LSA  
64 involves melting of subduction modified peridotite as originally proposed by Defant and  
65 Drummond (1990). In contrast, the HSA are proposed to be analogues of the late Archean  
66 tonalite-trondjemite-granodiorite (TTG) magmas and derived from partial melts of  
67 subducted basaltic crust in the garnet stability field, which reacted with peridotite during  
68 ascent (Martin et al., 2005). Archean rocks with an “adakitic” geochemical signature have  
69 been used to argue in favour of a plate tectonics regime in the Archean (e.g. Martin, 1999;  
70 Polat and Kerrich, 2001; Many et al., 2007; Manykamba et al., 2007; Mohan et al., 2013;  
71 Kwelwa et al., 2013).

72 Alternative models for rocks with an “adakitic” signature have been proposed, and  
73 involve fractional crystallization in the garnet stability field (e.g. Kamber et al., 2002;  
74 Macpherson et al., 2006; Richard and Kerrich, 2007; Rooney et al., 2011), by melting of  
75 thickened mafic lower crust (e.g. Atherton and Petford, 1993; Rudnick, 1995; Wang et al.,  
76 2005), or through the interaction of delaminated eclogitic lower crust with the underlying  
77 mantle (e.g. Bedard et al., 2003; Tulloch and Kimbrough, 2003; Gao et al., 2004; Wang et al.,  
78 2005; Goss et al. 2011). Since most of the continental crust was formed in the Archean (e.g.  
79 Taylor and McLennan, 1995; Tatsumi, 2008; Hacker et al., 2015) and the Archean rock record  
80 is dominated by rocks with an adakite-like (TTG’s; e.g. Condie, 2005; Moyen, 2011; Moyen  
81 and Martin, 2012) geochemical signature, understanding the petrogenetic processes that  
82 resulted in the formation of rocks with an adakitic signature in the Archean is essential. This  
83 is particularly important for the late Archean period when major shifts in the composition of  
84 the TTG suites are interpreted to reflect fundamental changes in global tectonics (e.g. Condie,  
85 2005; Martin et al., 2010; Moyen and Martin, 2012; Condie, 2014). In this contribution we  
86 present major and trace element geochemical data from the Kukuluma Intrusive Complex  
87 (KIC) that intruded the Neoproterozoic Geita Greenstone Belt of NW Tanzania and discuss the  
88 petrogenesis of the KIC, and the implications of this for the tectonic evolution of the Geita  
89 Greenstone Belt.

## 90 **Regional geology**

91 From a geological perspective, the Tanzania Craton was initially divided in three  
92 major litho-stratigraphic units: the Dodoman, the Nyanzian and the Kavirondian Supergroups  
93 (e.g. Stockley, 1936; Quennel et al., 1956; Harpum, 1970; Gabert, 1990). The Dodoman was  
94 interpreted to represent the basement to the Nyanzian, while the Kavirondian unconformably  
95 overlays the Nyanzian. The Dodoman consists of high-grade mafic and felsic granulite with

96 subordinate lower-grade schist and thin slivers of greenstone; the Nyanzian consists of mafic  
97 and felsic volcanics, ironstone, tuff and epiclastic sediments, while the Kavirondian consists  
98 of conglomerate, quartzite, grit, sandstone and siltstone. Borg and Krogh (1999) have shown  
99 that migmatitic gneisses, dated at  $2680 \pm 3$  Ma, that occur in the northern part of the Tanzania  
100 Craton are much younger than the Dodoman age units (interpreted to be  $\geq 3000$  Ma in age),  
101 and, therefore, cannot represent basement units. This was later confirmed by Chamberlain  
102 and Tosdal (2017), Kabete et al (2012) and Sanislav et al. (2014), who reviewed the existing  
103 geochronological data for the entire Tanzania Craton and concluded that there is no evidence  
104 of Dodoman age rock units in the northern half of the Tanzania Craton. Kabete et al. (2012),  
105 based on geophysical interpretation and limited field observations, divided the Tanzania  
106 Craton into a series of NW trending, shear-zone bounded accretionary terranes; they  
107 subdivided northern Tanzania (Fig. 1) into the Lake Nyanza Superterrane, Mwanza-Lake  
108 Eyasi Superterrane and the East Lake Victoria Superterrane.

109 The geology of the northern half of the Tanzania Craton is dominated by granite,  
110 gneiss and greenstone belts. Borg and Shackleton (1997) identified six greenstone belts: the  
111 Musoma-Mara, Kilimafedha, Iramba-Sekenke, Shinyanga-Malita, Nzega and Sukumaland  
112 greenstone belts. Although these greenstone belts share some common geological features,  
113 differences in age and geochemical signature between the individual greenstone belts indicate  
114 that their stratigraphy and geological evolution must be treated separately (e.g. Manya et al.,  
115 2007; Manya and Maboko, 2008).

116 The Sukumaland Greenstone Belt comprises a series of individual greenstone  
117 fragments separated by shear zones and granitoid intrusions. These fragments appear to share  
118 common stratigraphic features (e.g. Borg et al., 1990; Borg, 1994) similar to the Nyanzian  
119 and Kavirondian Supergroups (Manya and Maboko, 2003), but each fragment is large enough  
120 to be defined as a greenstone belt in its own right (Cook et al., 2015). The Nyanzian

121 Supergroup in the Sukumaland Greenstone Belt was subdivided into Lower and Upper  
122 Nyanzian (Manya and Maboko, 2003). The Lower Nyanzian is dominated by tholeiitic mafic  
123 volcanics with minor felsic volcanics and shale. Sm-Nd whole rock model ages (e.g. Manya  
124 and Maboko, 2003; Manya and Maboko, 2008; Cook et al., 2015) indicate that the mafic  
125 volcanics of the Lower Nyanzian in the Sukumaland Greenstone Belt were erupted at ca.  
126 2820 Ma. Based on their similar eruption ages, geochemistry and Nd isotopic signature the  
127 mafic volcanics of the lower Nyanzian have been grouped into the Kiziba Formation (Cook et  
128 al., 2015) that was interpreted to have formed in an oceanic plateau-like environment. The  
129 Kiziba Formation has been metamorphosed to lower amphibolite facies (Cook et al., 2015).  
130 The Lower Nyanzian is overlain by the Upper Nyanzian, which is composed of shale,  
131 volcanoclastics, ironstone, chert, sandstone, siltstone and mudstone (Borg et al., 1990; Borg,  
132 1994). In the Geita Greenstone Belt (GGB, Sanislav et al., 2014), which forms the northern  
133 part of the Sukumaland Greenstone Belt (Fig. 1), the contact between the mafic volcanics of  
134 the Kiziba Formation and the Upper Nyanzian is marked by a major shear zone (Cook et al.,  
135 2015). The entire sequence is complexly deformed with eight deformation events identified  
136 in the Upper Nyanzian sequence that hosts the Nyankanga, Geita Hill and Matandani-  
137 Kukuluma gold deposits in the GGB (Sanislav et al., 2015, 2017; Figs 1, 2). The Kavirondian  
138 Supergroup (Manya and Maboko, 2003) occurs as isolated outcrops that unconformably  
139 overly the Upper Nyanzian and is composed of conglomerate, grit, quartzite and sandstone  
140 (e.g. Borg et al., 1990; Borg, 1992, 1994).

141 The northern part of the GGB is intruded by 2620-2660 Ma (Sanislav et al., 2014)  
142 high-K granite batholiths while the southern part of the GGB is bordered by gneiss from  
143 which it is separated by a ductile shear zone. The eruption of the mafic volcanics forming the  
144 Kiziba Formation in the GGB was dated at ~ 2820 Ma (Manya and Maboko, 2008; Cook et  
145 al., 2015), whilst the maximum depositional age for the Upper Nyanzian sediments has been

146 variably given as 2771 (Chamberlain and Tosdal., 2007) and 2702 Ma (Sanislav et al., 2014).  
147 Borg and Krogh (1999) dated a diorite sill (Sanislav et al., 2015) that intruded the ironstones  
148 in the Geita Hill deposit at  $2699\pm 9$  Ma confirming that the sedimentation of the Upper  
149 Nyanzian in the Geita Greenstone Belt probably ceased by  $\sim 2700$  Ma. Detailed mapping  
150 (Sanislav et al., 2015, 2016) around the Nyankanga and Geita Hill gold deposits indicate that  
151 the Upper Nyanzian sediments experienced an early extensional shearing event ( $D_1$ ) followed  
152 by four compressional folding events ( $D_2$ - $D_5$ ) and three transpressional to transtensional  
153 brittle-ductile shearing events along discrete shear zones ( $D_6$ - $D_8$ ). Zircon ages from intrusive  
154 porphyries within the greenstone belt and the surrounding granite constrain all tectonic  
155 activity between 2820 and 2620 Ma (Manya and Maboko, 2008; Sanislav et al., 2014).

### 156 **Petrographic description of the Kukuluma Intrusive Complex**

157 The Kukuluma Intrusive Complex (KIC) consists of a series of NW trending  
158 intermediate igneous rocks (Fig. 2) that intruded the folded sequence of the Upper Nyanzian  
159 sediments, during the  $D_2$ - $D_3$  compressional stages affecting the GGB, sometime between  
160 2680-2700 Ma (Kwelwa, 2017). Three major gold deposits, Matandani, Kukuluma and Area  
161 3 W, occur along the contact between the KIC and the sediments (Fig. 2). The KIC is  
162 dominated by equigranular, fine- to medium-grained and locally porphyritic, intermediate  
163 intrusives (Fig. 3) and subordinate felsic (Fig. 3) porphyritic dykes.

164 The intermediate intrusive bodies are weakly to moderately foliated, indicating syn-  
165  $D_3$  emplacement (using the deformation scheme of Sanislav et al., 2015). The mineralogy is  
166 dominated by plagioclase (30-45 %), amphibole (30-40 %), alkali-feldspar (5-25 %), biotite  
167 (5-15%) pyroxene (5-10%) and quartz (5-20%). Based on the mineralogical composition the  
168 intermediate intrusives of the KIC can be separated into a diorite suite (gabbro-diorite and  
169 diorite; Figs. 3a and b) and a monzonite suite (monzodiorite and monzonite; Figs. 3c and d).



170 The feldspars are only partly sericitized (Figs. 3b and d) while some of the mafic minerals are  
171 partly replaced by metamorphic actinolite. Accessory minerals include apatite, magnetite, and  
172 rutile. Minor chlorite and carbonate are present as disseminated minerals, partly replacing  
173 the mafic minerals or along veins.

174 The felsic porphyritic dykes (Figs. 3e and f) show a narrower variation in their  
175 mineralogical composition. Their mineralogy is dominated by quartz (15-40 %), plagioclase  
176 (50-70%), K-feldspar (5-40%), biotite (5-15%) and amphibole (1-10%). The main accessory  
177 minerals are apatite and zircon. Based on their mineralogical composition the felsic phase of  
178 the KIC varies between granodiorite and tonalite. The plagioclase is partly sericitized and the  
179 mafic minerals are partly replaced by chlorite.

## 180 **Methodology for major and trace element analyses**

181 Whole rock geochemical analyses were performed at the Advanced Analytical Centre  
182 at James Cook University (JCU) on samples collected from drill core. All samples were  
183 collected away from the mineralized zones to minimize the effect of alteration. All samples  
184 were studied under the petrographic microscope and only samples that showed the minimum  
185 alteration were selected for further analyses. Approximately 1 kg of material was milled from  
186 each sample to a fine powder in a tungsten carbide ring mill. Major elements were analysed  
187 by conventional X-ray fluorescence (XRF) using a Bruker-AXS S4 Pioneer XRF  
188 Spectrometer on fused beads. The fused beads were prepared from rock powders mixed with  
189 12:22 borate flux (XRF Scientific Limited, Perth, Australia) at 1:8 sample to flux ratio that  
190 were fused to glass after heating to 1050 °C in a F-M 4 Fusion Bead Casting Machine  
191 (Willunga, Australia). Chips of the fused beads were mounted into a standard epoxy puck and  
192 analysed for a range of trace elements using a Geolas Pro 193 nm ArF Excimer laser ablation  
193 unit (Coherent) coupled to a Varian 820 quadrupole ICP-MS. Helium was used as the carrier

194 gas (0.8 l/min), which was subsequently mixed with Ar via a mixing bulb between the  
195 ablation cell and the ICP-MS to smooth the ablation signal. Laser energy density was set to 6  
196 J/cm<sup>2</sup>, and the laser spot size and repetition rate were set to 120 µm and 10 Hz, respectively.  
197 Each fused bead was analysed 3 times and average values are reported. The ICP-MS was  
198 tuned to ensure robust plasma conditions and low oxide production levels ( $\leq 0.5\%$  ThO) with  
199 the plasma power set at 1.25 kW. NIST SRM 610 glass was used as a bracketed external  
200 standard using the standard reference values of Spandler et al. (2011). Data were quantified  
201 using Ca (as previously determined by XRF on the same fused bead) as the internal standard,  
202 and data were processed using the Glitter software (Van Achterbergh et al., 2001). To  
203 monitor precision and accuracy of the analyses, we analysed Hawaiian basalt reference glass  
204 (KL2-glass; n=21) as a secondary standard (Jochum et al., 2006). The precision for REE  
205 analyses by LA-ICP-MS is better than 5% (mostly <3%), and the accuracy is often <2%. The  
206 standard reference material NIST612 (n=11) was analysed as a ternary standard. The  
207 precision for all the elements, besides Zn (3.5%) and Ge (~8.3%), is <2%, and <1% for REE.  
208 The accuracy for all the elements (standard reference concentrations taken from Spandler et  
209 al., 2011) is <3%. The only exceptions are Tb (6.5%), Ge (~8.3%), Sb (~9%), and Zn  
210 (~5.3%) where relatively large uncertainties in the NIST612 glass have to be taken into  
211 consideration.

## 212 **Alteration and element mobility**

213 The KIC rocks are deformed, metamorphosed and locally overprinted by hydrothermal  
214 alteration related to gold mineralisation concentrated along its margins. The top 100 meters  
215 of the intrusive complex is highly weathered so that all samples were collected from diamond  
216 drill holes that intercepted the intrusive complex at more than 400 meters below the surface,  
217 and away from mineralised zones. Petrographic examination of the samples revealed minor

218 carbonate and chlorite alteration indicating that the samples have been hydrated and  
219 carbonated. The loss of ignition (LOI) values of up to 5.5% confirms the petrographic  
220 observations and requires that all samples be screened for element mobility. On the alteration  
221 boxplot of Large et al. (2001), which combines the alteration index of Ishikawa  
222  $(100(K_2O+MgO)/(K_2O+MgO+Na_2O+CaO))$  and the chlorite-carbonate-pyrite alteration  
223 index  $((100(MgO+FeO))/(MgO+FeO+Na_2O+K_2O))$ , all samples plot (Fig. 4a) into the field of  
224 least altered rocks. However, to further test the element mobility for the KIC samples we  
225 used only the monzonite and diorite suites, because the higher number of samples allows  
226 compositional variations induced by post-magmatic alteration to be identified more easily.  
227 Na, K, Rb and Sr are all easily mobilised during low-temperature hydrothermal alteration and  
228 metamorphism. The post-magmatic disturbance of Na, K, Rb and Sr by hydrothermal  
229 alteration and metamorphism can be tested by plotting their concentration against the LOI  
230 values. A lack of correlation indicates little or no significant disturbance while well-  
231 correlated trends indicate significant disturbance and mobility (e.g. Papoulis et al., 2004;  
232 Harvey et al., 2014). The lack of any correlation between these elements and the LOI values  
233 (Fig. 4b, c, d and e) combined with their coherent behaviour on other geochemical plots  
234 suggests that the post-magmatic alteration did not significantly mobilise these elements, and  
235 they can, therefore, be used for petrogenetic interpretations. In general REE and HFSE are  
236 considered immobile during hydrothermal alteration and greenschist facies metamorphism,  
237 but situations where the REE were mobile have been documented (e.g. Wood et al., 1976;  
238 Condie et al., 1977); with the LREE considered to be more mobile than the HREE (Sun and  
239 Nesbit, 1978). To test the mobility of the REE from the KIC rocks, we plotted the  
240 concentration of La against Zr (Fig. 4f), and to test the mobility of the HFSE we plotted the  
241 concentration of Nb against Zr (Fig. 4g). The strong positive correlation that exists between  
242 these elements in combination with the coherent behaviour of the REE and HFSE on

243 chondrite and primitive mantle normalised plots indicate that these elements most probably  
244 retained their original concentrations. The ratio of highly incompatible elements such as Th  
245 and U should be near chondritic ( $\text{Th}/\text{U}_{\text{chondrite}} = 3.63$ ; Sun and McDonough, 1989) unless  
246 disturbed by alteration processes when U is mobile under oxidizing conditions. The average  
247 Th/U ratio of all KIC rocks ( $\text{Th}/\text{U}_{\text{monzonite}} = 3.65$ ;  $\text{Th}/\text{U}_{\text{diorite}} = 2.92$ ;  $\text{Th}/\text{U}_{\text{granodiorite}} = 2.92$ ) is near  
248 chondritic suggesting little to no mobility of these elements during hydrothermal alteration  
249 and metamorphism.

### 250 **The geochemistry of the KIC**

251 The geochemical composition of the KIC (Table 1 and Fig. 5) is characterised by:  
252 intermediate  $\text{SiO}_2$  (59.17 wt%), moderate #mg (0.47), high  $\text{Al}_2\text{O}_3$  and FeO (15.83 wt% and  
253 5.66 wt% respectively) and moderate MgO (2.78 wt%). The  $\text{K}_2\text{O}/\text{Na}_2\text{O}$  ratio is less than 1  
254 (0.70) and  $\text{CaO} + \text{Na}_2\text{O}$  is more than 8 (8.82%). The Y content is low (14.5 ppm) and Sr is  
255 high (765 ppm) with an average Sr/Y ratio of 59. The HREE are depleted relative to the  
256 LREE with an average La/Yb ratio of 42 and the Cr content is moderately high (62 ppm). The  
257 chondrite normalized REE pattern (Fig. 6) show fractionated patterns while the primitive  
258 mantle normalized multi-element patterns show negative Nb and Ti anomalies and a general  
259 enrichment in the large ion lithophile elements (LILE).

### 260 **The monzonite suite**

261 The geochemical composition of rocks that belong to the monzonite suite (Fig. 5;  
262 Table 1) from the KIC is characterized by intermediate  $\text{SiO}_2$  (51.7- 62.1 wt%), FeO (3-9  
263 wt%), MgO (2.5-5.6wt%) and CaO (3.8-7 wt%), moderate  $\text{K}_2\text{O}$  (0.9-3.6 wt%), high  $\text{Al}_2\text{O}_3$   
264 (14.4-16.5 wt%) and  $\text{Na}_2\text{O}$  (4.5-6.6 wt%) and low  $\text{TiO}_2$  (0.4-0.6 wt%). They have high  
265  $\text{CaO} + \text{Na}_2\text{O}$  (8.6-12.9), high Sr (537-1563 ppm) and high LREE ( $\text{La}_n = 241-777$  ppm; the  
266 subscript “n” refers to chondrite normalized). These features combined with a low  $\text{K}_2\text{O}/\text{Na}_2\text{O}$

267 ratio (0.1-0.8), low Y (11-30 ppm), low HREE ( $Yb_n = 4-11$ ) and high Sr/Y and La/Yb ratios  
268 (30-119 and 67-102 respectively) indicate that the monzonite suite has geochemical  
269 characteristics similar to adakites, sanukitoids and Closepet-type granite. Martin et al (2005)  
270 suggested that less differentiated sanukitoids ( $SiO_2 < 62$  wt%) are similar to LSA and  
271 Closepet-type granite. However, rocks that belong to the monzonite suite from the KIC have,  
272 on average, higher Y, Yb and La/Yb than the LSA, higher #mg, Sr, Cr, Sr/Y and La/Yb than  
273 the Closepet-type granite, and higher La/Yb than the average sanukitoid. At the same time  
274 the monzonite suite has lower  $TiO_2$ , #mg, Sr, Cr, Ni and Sr/Y than the LSA, lower  $TiO_2$ , Y,  
275 Yb than the Closepet-type granite and lower Cr compared to the average sanukitoid. The  
276 chondrite normalized REE pattern (Fig. 6a) of monzonite suite rocks is subparallel to the  
277 pattern from average LSA, sanukitoid and Closepet-type granite and shows the strong LREE  
278 enrichment characteristic for these type of rocks. When plotted on a primitive mantle  
279 normalized multielement diagram (Fig. 6b) the monzonite suite shows strong negative  
280 anomalies for Nb and Ti, and moderate negative anomalies for Zr and Sr. Their pattern is  
281 subparallel to that of the LSA, sanukitoids and Closepet-type granite. Notable differences are  
282 the positive Sr anomaly for the LSA, the lack of a Sr anomaly in sanukitoids and the lack of a  
283 negative Zr anomaly in LSA, sanukitoids and Closepet-type granite.

#### 284 **The diorite suite**

285 Rocks that belong to the diorite suite (Fig. 5; Table 1) have similar  $SiO_2$  (53-63 wt%)  
286 contents compared to monzonite suite rocks, but slightly higher  $Al_2O_3$  (14.4-17.1 wt%), FeO  
287 (2.8-7.8 wt%), and  $TiO_2$  (0.3-0.7 wt%), and slightly lower  $Na_2O$  (3.1-5.6 wt%),  $K_2O$  (1.2-3.2  
288 wt%) and  $P_2O_5$  (0.1-0.3 wt%). These values combined with  $K_2O/Na_2O \sim 0.54$ ,  $CaO+Na_2O \sim$   
289 8, low Y (8-12 ppm), low HREE ( $Yb_n = 3-7$  ppm) and high Sr (572-1062 ppm), Cr (49-99  
290 ppm) and LREE ( $La_n = 45-161$  ppm) suggest that the diorite suite also shares geochemical  
291 features with sanukitoid, adakite and Closepet-type granite. The average composition of



292 rocks from the diorite suite is similar to the average composition of HSA except for lower  
293  $\text{SiO}_2$  (58.6 vs 64.8), higher FeO (6.39 vs. 4.27), higher Cr (75 vs 41) and higher Sr/Y (85 vs  
294 56). The chondrite normalized REE pattern (Fig. 6c) is similar to the average HSA and  
295 subparallel to, but at lower concentrations than the average LSA, sanukitoid and Closepet-  
296 type granite. On a primitive mantle normalized multi-element diagram (Fig. 6d) diorite suite  
297 rocks show pronounced negative Nb anomalies, moderately negative Ti anomalies and  
298 moderately positive Sr anomalies, all of which are also typical for LSA. The overall pattern is  
299 similar to that of HSA, except for the positive Sr anomaly, and is subparallel to the average  
300 pattern of LSA, sanukitoid and Closepet-type granite, but at lower concentrations.

### 301 **The granodiorite suite**

302 Four samples from the KIC were classified as granodiorites. Although the samples  
303 were collected a few hundred meters apart their major and trace element composition is  
304 almost identical (Fig. 5; Table 1). They have moderate  $\text{SiO}_2$  (av. 62.5 wt%), low FeO (av. 4.9  
305 wt%), MgO (av. 1.9 wt%), CaO (av. 3.7 wt%) and high  $\text{K}_2\text{O}$  (av. 3.67 wt%) when compared  
306 to rocks from the monzonite and the diorite suite. Their  $\text{K}_2\text{O}/\text{Na}_2\text{O}$  ratio is high (av. 1.1),  
307  $\text{CaO}+\text{Na}_2\text{O}$  is low (av. 7.4), Y is low (16 ppm), HREE are low ( $\text{Yb}_n = 10$ ), LREE are  
308 moderately high ( $\text{La}_n = 100$  ppm), and Sr and Cr content are relatively high (332 and 21 ppm  
309 respectively). The lower Sr content (< 400 ppm), a Sr/Y ratio of less than 40 and a La/Yb  
310 ratio of less than 20 suggest that the granodiorites cannot be considered to have an adakite-  
311 like signature sensu Defant and Drummond (1990). However, as pointed out by Moyen  
312 (2009), HSA can have a Sr/Y ratio as low as 20. On a chondrite normalized REE diagram  
313 (Fig. 6e) the granodiorites display a subparallel trend to that of the HSA but they plot at  
314 higher concentrations. They also show a weak negative Eu anomaly indicative of plagioclase  
315 fractionation. On a primitive mantle normalized multi-element diagram (Fig. 6f) their pattern

316 is similar to that of the HSA, except that they have a weak negative Sr anomaly while the  
317 HSA have a weak positive Sr anomaly.

## 318 **Petrogenesis of the KIC**

### 319 **Relative timing of emplacement**

320 Rocks of the granodiorite suite have been dated at 2651 Ma to 2667 Ma (Kwelwa,  
321 2017), but there are no direct age data available for rocks forming the monzonite and diorite  
322 suites. However, field relationships help constrain their relative timing of emplacement. The  
323 intrusives of the monzonite and diorite suites occur as a series of intrusive bodies subparallel  
324 to the NW-SE trending regional fabric (Fig. 2). The rocks contain a weakly to well-developed  
325 foliation that is subparallel to the axial planar surface of regional D<sub>3</sub> folds (Sanislav et al.,  
326 2015, 2017) indicating coeval and syntectonic emplacement. The granodiorite suite rocks are  
327 not foliated indicating that their emplacement postdates the emplacement of the diorite and  
328 the monzonite suite. Felsic dykes similar in composition to the granodiorite suite outcrop in  
329 the Kukuluma and Matandani deposits where they crosscut the folded sequence and are  
330 crosscut by brittle ductile shear zones.

331 In the Nyankanga and Geita Hill areas, monzonite and diorite dykes and sills intrude  
332 during D<sub>2</sub> and D<sub>3</sub>, i.e. at a time relative to deformation that is near identical to the relative  
333 timing observed in Kukuluma (Sanislav et al., 2015, 2017). Borg and Krogh (1999) provide  
334 an age of 2699±9 Ma for a diorite dyke from Geita Hill, and Chamberlain and Tosdal (2007)  
335 report an age of 2698±14 Ma for diorite in the Nyankanga pit where it has been cross cut by  
336 several generations of felsic dykes dated at 2685-2696 Ma (Chamberlain and Tosdal, 2007).  
337 Therefore, by comparison, the monzonite and diorite suites of the KIC are interpreted to have  
338 been emplaced between 2685-2700 Ma.

339 **Depth and source of melts**

340 Fractionated REE patterns (Fig. 6), high Sr/Y and La/Yb ratios (Figs. 7a and b), and  
341 low Y and Yb contents suggest that garnet was present as a fractionating or residual phase in  
342 the melt (e.g. Martin et al., 2005; Moyen, 2009; Castillo, 2012). However, high Sr/Y and  
343 La/Yb ratios can also reflect an enriched source (Moyen, 2009), can be produced by the  
344 fractionation of amphibole, and by the delayed crystallization of plagioclase in hydrous mafic  
345 magmas (Castillo, 2012), while fractionated REE patterns may result from amphibole  
346 fractionation (e.g. Romick et al., 1992; Richards and Kerrich 2007). Continental crust has  
347 high Sr/Y and La/Yb ratios, therefore, melting of continental crust and/or mixing with  
348 continental crust may impart high Sr/Y and La/Yb to their derivative melts. The low SiO<sub>2</sub> and  
349 moderate Mg# of the KIC rocks suggest a mafic to ultramafic source, and preclude any  
350 significant contribution from felsic rocks. In mafic melts fractionation of amphibole may  
351 increase the La/Yb ratio of the residual melt, but the REE pattern will not develop a strongly  
352 concave shape. As magma becomes more dacitic the hornblende REE distribution  
353 coefficients increase and magmas develop concave REE patterns and high La/Yb ratios  
354 (Romick et al., 1992). So the net effect of amphibole and plagioclase fractionation is an  
355 increase in La/Yb and decrease in Dy/Yb (Moyen, 2009), whereas garnet fractionation or  
356 partial melting with residual garnet will increase the Dy/Yb ratio in the melt (e.g.  
357 Macpherson et al., 2006; Davidson et al., 2007). Kelemen et al. (2003) proposed that melts  
358 with a clear garnet (eclogite) signature should have Dy/Yb<sub>n</sub> ratios  $\geq 1.5$ . All samples of the  
359 monzonite suite and the majority of the diorite suite samples have Dy/Yb<sub>n</sub> > 1.5 (Fig. 7c)  
360 suggesting that their high Sr/Y and La/Yb ratios are related to deep melting. Eclogite melts  
361 reacting with the mantle (Kelemen et al., 2003) would decrease both the Dy/Yb and the  
362 La/Yb ratios (Fig. 7d) of the initial melt. Therefore, a lack of eclogite melting signature in  
363 some of the samples (i.e. the granodiorite suite) does not automatically rule out their

364 derivation from eclogite/garnet-bearing melts. Moreover, plagioclase crystallization can  
365 decrease Sr/Y ratios and increase Y concentrations. Thus, a deep melting signature (based on  
366 this ratio) can be erased by large degrees of plagioclase fractionation (e.g. Richard and  
367 Kerrich, 2007).

368 The major element variation diagrams show that for the same SiO<sub>2</sub> content (Fig. 5),  
369 the diorite and the monzonite suites display subparallel trends for most of the elements. It is  
370 particularly obvious for Al<sub>2</sub>O<sub>3</sub>, FeO<sub>t</sub>, Na<sub>2</sub>O, TiO<sub>2</sub> and P<sub>2</sub>O<sub>5</sub>. Assuming that the two suites  
371 were derived from rocks having a similar composition this subparallel evolution of the major  
372 elements cannot be explained by magma mixing or by fractional crystallization alone and  
373 requires melting at different pressures. For example, the Al<sub>2</sub>O<sub>3</sub> content of melts becomes  
374 depleted with increasing pressure at the same degree of partial melting (e.g. Hirose and  
375 Kushiro, 1993; Spandler et al., 2008). The negative correlation between SiO<sub>2</sub> and Al<sub>2</sub>O<sub>3</sub> (Fig.  
376 5a) in the diorite suite may indicate garnet fractionation or residual garnet, which will  
377 effectively reduce Al<sub>2</sub>O<sub>3</sub> with increasing SiO<sub>2</sub> in the melt (Macpherson et al., 2006; Davidson  
378 et al., 2007). The positive correlation observed in the monzonite suite may indicate that  
379 garnet was partly consumed during melting. The monzonite suite rocks tend to have higher  
380 Na<sub>2</sub>O at the same CaO (Fig. 8a) compared to the diorite suite rocks. This can also indicate a  
381 higher pressure during melting as Na<sub>2</sub>O becomes more compatible in clinopyroxene at higher  
382 pressure (e.g. Kogiso et al., 2004).

383 On chondrite normalized diagrams (Fig. 6) the REE patterns for the two suites are  
384 subparallel, but the LREE elements are more fractionated for the monzonite suite than the  
385 diorite suite. This is also illustrated by much higher La/Yb<sub>n</sub> and Dy/Yb<sub>n</sub> ratios (Fig. 7)  
386 suggesting that rocks belonging to the monzonite suite may represent deeper melts compared  
387 to rocks from the diorite suite. Their primitive mantle normalized trace element patterns (Fig.  
388 6) are also sub-parallel, with the notable difference that the diorite suite rocks have a positive

389 Sr anomaly while the monzonite suite rocks have negative Sr and Zr anomalies. The presence  
390 of a significant positive Sr anomaly in the diorite suite cannot be explained by melting or  
391 crystallization unless plagioclase is involved. The lack of any correlation between the Sr/Sr\*  
392 and the MgO (Fig. 8b) excludes fractionation. Thus, a plagioclase-rich component is required  
393 in the melt source region. Alternatively, interaction of the melt with a plagioclase-rich region  
394 (assimilation) will produce a similar effect. However, assimilation will result in a large  
395 decrease in FeO<sub>t</sub> and a large increase in Al<sub>2</sub>O<sub>3</sub> with decreasing MgO (e.g. Peterson et al.,  
396 2014), which is not the case here. Therefore assimilation can be excluded.

397 The only viable explanation is that the positive Sr anomaly is related to the source  
398 rock. We propose that the diorite suite was formed by melting of garnet-bearing amphibolite  
399 and plagioclase was completely transferred into the melt, leaving behind a Sr-depleted  
400 (relative to Ce and Nd) residue of garnet-clinopyroxene-rutile eclogite. Further melting of the  
401 eclogite with residual rutile produced the monzonite suite with negative Sr and Zr anomalies.  
402 Zr and Hf have similar chemical properties and should not fractionate from each other in  
403 geological processes; i.e. their ratio should be chondritic in all earth materials (e.g.  
404 Zr/Hf= $\sim$ 36.3; Sun and McDonough, 1989). The diorite suite has an average Zr/Hf ratio of  
405 36.8 (Fig. 8c), which is similar to the chondritic value, but the monzonite suite has an average  
406 Zr/Hf ratio of 42.7 (Fig. 8c), which exceeds the chondritic value suggesting that these  
407 elements were fractionated from each other. Experimental data on amphibole/melt partition  
408 coefficients (e.g. Foley et al., 2002; Tiepolo et al., 2007) have shown that amphibole can  
409 fractionate most HFSE causing negative Ti and Nb anomalies, but only high-Mg amphibole  
410 can fractionate Zr from Hf. The ability of garnet to fractionate Zr from Hf is dependent on  
411 pressure and MgO content (e.g. Green et al., 2000; van Westrenen et al., 1999). The only  
412 mineral able to effectively fractionate HFSE from each other is rutile (Stalder et al., 1998;  
413 Foley et al., 2000). If rutile was the residual phase, the Nb/La and Zr/Sm ratios of the melt



414 will correlate positively (Münker et al., 2004), but if high-Mg amphibole was the residual  
415 phase the melt ratios of these elements will correlate negatively. The monzonite suite shows a  
416 clear positive correlation between Nb/La and Zr/Sm (Fig. 8d) implying residual rutile.  
417 However, the diorite suite shows no correlation between these two ratios. Rutile cannot  
418 coexist with basaltic melts arising from the partial melting of peridotite (e.g. Ryerson and  
419 Watson, 1987; Woodhead et al., 1993; Thirlwall et al., 1994), because it reacts with the  
420 olivine to form orthopyroxene and ilmenite. Thus, the most likely source for the monzonite  
421 suite is rutile-bearing, garnet-clinopyroxene eclogite.

### 422 **Melt mantle interaction**

423 The low SiO<sub>2</sub> content, average Mg numbers, and relatively high Ni and Cr  
424 concentrations indicate that the source rocks for the KIC must be mafic or ultramafic. Their  
425 intermediate composition (SiO<sub>2</sub> ≤ 62 wt%) suggests that fractionation played a minor role in  
426 their petrogenesis and they are close to primary magmas. From this point of view the rocks of  
427 the KIC resemble LSA and sanukitoid. However, there are some important differences.  
428 Firstly, at the same SiO<sub>2</sub> content the rocks of the KIC have much lower MgO compared to  
429 LSA (Fig. 5b). Secondly, the rocks of the KIC overlap the field of mafic experimental melts  
430 (Figs 3a,b and f), whereas LSA rocks plot above it, and the sanukitoids overlap with it, but  
431 only for low MgO concentrations. Because of their low SiO<sub>2</sub>, high Mg numbers and high Cr  
432 and Ni concentrations, the LSA and the sanukitoids are commonly interpreted to have formed  
433 by partial melting of mantle peridotite metasomatised by felsic melts (e.g. Shirey and  
434 Hanson, 1984; Rapp et al., 1999; Martin et al., 2005). The rocks of the KIC have lower Mg  
435 numbers (at the same SiO<sub>2</sub> content; Fig. 5b) and much lower Cr, Ni, Sr, K, Rb and Nb  
436 concentrations compared to LSA rocks and the sanukitoids (Fig. 9 and Table 1). The  
437 difference between KIC rocks and LSA rocks is clearly illustrated in Figure 9 where the

438 composition of KIC rocks overlaps the composition of the HSA, and closely resembles the  
439 composition of experimental melts of basalt (Figs. 7a and b).

440 On the K vs Rb diagram (Fig. 9a) some of the LSA rocks plot subparallel to the Y-axis  
441 suggesting high K/Rb ratios, which were interpreted to reflect Rb depletion by selective  
442 melting of metasomatic amphibole in a peridotite source (e.g. Martin et al., 2005 and  
443 references therein). However, in the absence of metasomatism, both peridotite and basaltic  
444 melts result in K/Rb ratios much lower than average oceanic basalt ( $K/Rb=1071$ ; Sun and  
445 McDonough, 1989). High Sr contents can reflect deep melting at pressures above the  
446 plagioclase stability field, melting of a source that was already high in Sr, and/or melt  
447 interaction with high-Sr geological materials (e.g. Moyen, 2009). Given the low  $SiO_2$  ( $\leq 62$   
448 wt%) of the KIC samples, their source rock must have been mafic or ultramafic.  
449 Experimental melting of basalt produced liquids with up to 1000 ppm Sr (Fig. 9b), but to  
450 achieve the high Sr observed in LSA, interaction with mantle peridotite is required (e.g.  
451 Martin et al., 2005). Rocks from the diorite and granodiorite suites plot within the fields of  
452 basaltic melts and HSA (Fig. 9b), while some of the samples from the monzonite suite plot at  
453 higher Sr values ( $\sim 1500$  ppm) within the field of LSA, which may indicate some level of  
454 interaction with mantle peridotite. However, if the source of the KIC rocks was mafic lower  
455 crust (Sr = 348 ppm; Rudnick and Gao, 2003; Sr = 289 ppm; Hacker et al., 2015) rather than  
456 an average oceanic basalt (Sr = 90 ppm; Sun and McDonough, 1989), than high Sr values  
457 observed in the monzonite suite do not necessarily require interaction with peridotite mantle.  
458 Maybe the most useful ratio to use when separating melts derived from partial melting of  
459 metasomatised mantle peridotite (LSA) and melts derived by partial melting of mafic rocks  
460 (HSA) is the Cr/Ni ratio (Fig. 9c; Martin et al., 2005). The Cr/Ni ratio for KIC samples (Fig.  
461 9c) is clearly distinct from that of the LSA and overlaps the field of the HSA suggesting a  
462 mafic source and minimum interaction with the mantle. The lack of correlation between the

463 Cr/Ni ratio and the Mg# (Fig. 9d) suggests that the Cr/Ni ratio of the KIC samples is a source  
464 characteristic and not dependent on fractionation.

### 465 **Tectonic setting**

466 The rocks of the KIC have major and trace element signatures similar to “adakitic”  
467 rocks. Although the original description of adakites (e.g. Defant and Drummond, 1990)  
468 specifically indicates that their geochemical signature is derived from partial melting of a  
469 subducted slab, it is clear now that high Sr/Y and La/Yb ratios alone cannot be used to  
470 unequivocally indicate a subduction setting (e.g. Moyen, 2009; Castillo, 2012), and rocks  
471 with an “adakitic” signature can form in different tectonic settings as well. The KIC was  
472 emplaced syn-tectonically along axial planar surfaces of upright regional folds suggesting a  
473 period of crustal thickening between 2685-2700 Ma. The age data from the northern half of  
474 the Tanzania Craton (e.g. Kabete et al., 2012; Sanislav et al., 2014) suggest that growth of  
475 this part of the craton started at ~ 2820 Ma with extensive tholeiitic mafic volcanism (e.g.  
476 Many and Maboko, 2003, 2008; Cook et al., 2015) followed by a period dominated by the  
477 intrusion of diorite and TTG and completed with the intrusion of the 2620-2660 Ma high-K  
478 granites (Sanislav et al., 2014). Thus, the KIC was emplaced during the transition period from  
479 higher depth TTG magmas to shallower depth high-K magmas.

480 Cook et al. (2015) proposed that the ~ 2820 Ma mafic volcanics (Kiziba Formation)  
481 that form the base of the stratigraphic sequence (Lower Nyanzian) in the Sukumaland  
482 Greenstone Belt were emplaced in an oceanic plateau like setting. However, it is unclear at  
483 the moment whether or not the Upper Nyanzian sediments (intruded by the KIC) were  
484 deposited on top of the Kiziba Formation or the two units were tectonically juxtaposed. In the  
485 Geita region the contact between the two units is structural (Cook et al., 2015), but there  
486 appears to be evidence that the Geita Greenstone Belt is underlain by the mafic rocks of the  
487 Kiziba Formation suggesting that crustal growth in this part of Tanzania occurred by partial

488 melting and maturation of an oceanic plateau by lower crustal delamination/modification  
489 (e.g. Vlaar et al., 1994; Zegers and van Keken, 2001; Bedard, 2006; Bedard et al., 2013;  
490 Cook et al., 2015). Chiaradia (2015) showed that there is a strong correlation between the  
491 Sr/Y ratio and MgO content of recent arc magmatism, and the upper plate thickness  
492 indicating that source processes (slab melting, slab melt-mantle interactions) do not play a  
493 major role in the generation of high Sr/Y signatures. This implies that high Sr/Y ratios occur  
494 at lower MgO content, suggesting that thicker crust favours magma evolution at deeper  
495 levels, thus Sr/Y increases steadily with magmatic differentiation (Fig. 10a). In contrast,  
496 Archean rocks show a sudden increase of the Sr/Y ratio between ~2.5 and ~0.5 wt% MgO  
497 (Fig. 10a) suggesting that, as opposed to modern arc lava, source processes control the Sr/Y  
498 ratio of Archean rocks (Chiaradia, 2015). Source processes may include partial melting in the  
499 garnet stability field of subducted mafic crust or partial melting of delaminated lower mafic  
500 crust.

501 To investigate a possible subduction component in the generation of the KIC rocks we  
502 use Th/U vs Zr/Hf ratios. Partial melting in the mantle wedge can be excluded, as detailed  
503 above, based on the presence of Nb and Ti depletion due to residual rutile, which cannot  
504 coexist with basaltic melts arising from the partial melting of peridotite (e.g. Ryerson and  
505 Watson, 1987; Woodhead et al., 1993; Thirlwall et al., 1994) because it reacts with the  
506 olivine to form orthopyroxene and ilmenite. Given the highly incompatible behaviour of Th  
507 and U, normal magmatic processes cannot significantly fractionate these elements from each  
508 other. U and Th are easily fractionated during surface processes, because of the higher  
509 mobility of U during weathering and under oxidizing conditions. Seafloor alteration and  
510 addition of slab fluids will lower the Th/U ratio while dehydration and addition of sediment  
511 melts will increase the Th/U ratio (e.g. Bebout, 2007). Figure 10b shows that the diorite and  
512 the granodiorite suites have almost MORB-like Th/U and Zr/Hf ratios, thus precluding a

513 subduction component. The monzonite suite has higher Zr/Hf ratios due to residual rutile (see  
514 above), and the Th/U ratio varies between the values for the lower mafic crust end-member of  
515 Hacker et al. (2015) and the values for the average lower continental crust of Rudnick and  
516 Gao (2003). Overall, the KIC shows a very narrow variation in Th/U ratios, which is more  
517 consistent with partial melting of the mafic lower crust than partial melting of a subducted  
518 oceanic crust.

519

## 520 **Conclusions**

521 In general Archean igneous rocks with adakite-like signature are interpreted to  
522 indicate a subduction setting. We have shown that although the rocks of the KIC can be  
523 easily classified as “adakites”, detail screening of their composition revealed important  
524 differences. Given the recognition that rocks with adakite-like signature can form in a variety  
525 of tectonic settings from non-unique petrogenetic processes requires a re-examination of the  
526 existing Archean datasets. Higher Archean geothermal gradients would have favoured the  
527 development of thicker lithospheric roots and partial to complete eclogitization of the mafic  
528 lower crust; the removal of the eclogitised crust by delamination would favour partial melting  
529 of the thickened lower crust to generate adakite-like rocks. This scenario is similar to the  
530 interpretation of the post-tectonic adakite-like rocks from the Tibetan Plateau with the main  
531 difference that the KIC is syn-tectonic. Alternatively, the KIC formed by partial melting of  
532 eclogitised mafic lower crust of an Archean oceanic plateau.

## 533 **Acknowledgments**

534 This study is part of a PhD study undertaken by the first author at James Cook University.  
535 SDK would like to thank James Cook University for waiving the tuition fees and Geita Gold



536 Mine for providing the research funding for this study. Craig Duvel, Hatari Mjinja and the  
537 exploration team from Geita Gold Mine are greatly acknowledged for all of their support  
538 during this project. Carl Spandler is acknowledged for reading an early version of the  
539 manuscript and providing some thoughtful comments. Detailed comments by two anonymous  
540 reviewers are greatly acknowledged for helping improve the quality of the manuscript.

## 541 **References**

- 542 Atherton, M.P., Petford, N., 1993. Generation of sodium-rich magmas from newly  
543 underplated basaltic crust. *Nature* 362, 144-146.
- 544 Bebout, G.E., 2007. Metamorphic chemical geodynamics of subduction zones. *Earth and*  
545 *Planetary Science Letters* 260, 373-393.
- 546 Bedard, J.H., 2006. A catalytic delamination-driven model for coupled genesis of Archaean  
547 crust and sub-continental lithospheric mantle. *Geochimica et Cosmochimica Acta* 70,  
548 1188-1214.
- 549 Bédard, J.H., Harris, L.B., and Thurston, P.C., 2013. The hunting of the snArc: Precambrian  
550 Research, 229, 20-48.
- 551 Borg, G., 1992. New aspects on the lithostratigraphy and evolution of the Siga Hills, an  
552 Archean granite–greenstone terrain in NW-Tanzania. *Z. Angew. Geol.* 38, 89–93
- 553 Borg, G., 1994. The Geita gold deposit in NW Tanzania. *Geology, ore petrography*  
554 *geochemistry and timing events. Geol. Jb. D* 100, 545–595.
- 555 Borg, G., Lyatuu, D.R., Rammlair, D., 1990. Genetic aspects of the Geita and Jubilee reef,  
556 Archean BIF-hosted gold deposits, Tanzania. *Geol. Rundsch.* 79, 355–371.

- 557 Borg, G., Shackleton, R.M., 1997. The Tanzania and NE-Zaire Cratons. In: de Wit, M.J.,  
558 Ashwal, L.D. (Eds.), Greenstone Belts. Oxford University Press, Oxford, pp. 608–619.
- 559 Borg, G., and Krogh, T., 1999. Isotopic age data of single zircons from the Archaean  
560 Sukumaland Greenstone Belt, Tanzania. *Journal of African Earth Sciences* 29, 301-  
561 312.
- 562 Castillo, P. R., 2012. Adakite petrogenesis. *Lithos* 134-135, 304-316.
- 563 Chamberlain, C.M., Tosdal, R.M., 2007. U–Pb geochronology of the Lake Victoria  
564 Greenstone Terrane, Tanzania. Mineral Deposit Research Unit The University of  
565 British Columbia (Research Program on World-class Gold Deposits and Advanced  
566 Exploration Projects Owned and/or Joint Ventured to Barrick Gold, Placer Dome,  
567 Anglo - Gold Ashanti, Resolute Mining NL as Main Sponsors.
- 568 Chiaradia, M., 2015. Crustal thickness control on Sr/Y signatures of recent arc magmas: an  
569 Earth scale perspective. *Scientific Reports* 5, 8115.
- 570 Condie, K.C., 2005. TTGs and adakites: are they both slab melts? *Lithos* 80, 33–44.
- 571 Condie, K.C., 2014. Growth of continental crust: a balance between preservation and  
572 recycling. *Mineral. Mag.* 78, 623–637.
- 573 Condie, K.C., Viljoen, M.J., and Kable, E.D.J., 1977. Effects of alteration on element  
574 distributions in Archaean tholeiites from the Barberton greenstone belt, South Africa.  
575 *Contributions to Mineralogy and Petrology* 64, 75-89.
- 576 Cook, Y.A., Sanislav, I.V., Hammerli, J., Blenkinsop, T.G., and Dirks, P.H.G., 2015. A  
577 primitive mantle source for the Neoproterozoic mafic rocks from the Tanzania  
578 Craton. *Geoscience Frontiers*-in press.

- 579 Davidson, J., Turner, S., Handley, H., Macpherson, C., Dosseto, A., 2007. Amphibole  
580 “sponge” in arc crust? *Geology* 35, 787–790.
- 581 Defant, M.J., Drummond, M.S., 1990. Derivation of some modern arc magmas by melting of  
582 young subducted lithosphere. *Nature* 347, 662–665.
- 583 Drummond, M.S., Defant, M.J., 1990. A model for trondhjemite–tonalite–dacite genesis and  
584 crustal growth via slab melting: Archaean to modern comparisons. *Journal of*  
585 *Geophysical Research* 95, 21503–21521.
- 586 Foley, S., Tiepolo, M., Vannucci, R., 2002. Growth of early continental crust controlled by  
587 melting of amphibolite in subduction zones. *Nature* 417, 837– 840.
- 588 Foley, S.F., Barth, M.G., Jenner, G.A., 2000. Rutile/melt partition coefficients for trace  
589 elements and an assessment of the influence of rutile on the trace element  
590 characteristics of subduction zone magmas. *Geochim. Cosmochim. Acta* 64, 933–938.
- 591 Gabert, G., 1990. Lithostratigraphic and tectonic setting of gold mineralization in the  
592 Archaean Cratons of Tanzania and Uganda, East Africa. *Precambrian Research* 46,  
593 59–69.
- 594 Gao, S., Rudnick, R.L., Yuan, H.L., Liu, X.M., Liu, Y.S., Xu, W.L., Lin, W.L., Ayerss, J.,  
595 Wang, X.C., Wang, Q.H., 2004. Recycling lower continental crust in the North China  
596 craton. *Nature* 432, 892–897.
- 597 Goss, A.R., Kay, S.M., Mpodozis, C., 2011. The geochemistry of a dying continental arc: the  
598 Incapillo Caldera and Dome Complex of the southernmost Central Andean Volcanic  
599 Zone (28°S). *Contributions to Mineralogy and Petrology* 161, 101–128.

- 600 Green, T.H., Blundy, J.D., Adam, J., Yaxley, G.M., 2000. SIMS determination of trace  
601 element partition coefficients between garnet, clinopyroxene and hydrous basaltic  
602 liquids at 2 – 7.5 GPa and 1080–1200 °C. *Lithos* 53, 165– 187.
- 603 Hacker, B.R., Kelemen, P.B., Behn, M.D., 2015. Continental lower crust. *Annual Review of*  
604 *Earth and Planetary Sciences* 43, 167–205.
- 605 Harpum, J.R., 1970. Summary of the geology of Tanzania: structure and geotectonics of the  
606 Precambrian. *Tanzania Geol. Surv. Mem.* 1 Part V, 58 pp.
- 607 Harvey, J, Savov, IP, Agostini, S., Cliff, R.A., and Walshaw, R., 2014. Si-metasomatism in  
608 serpentized peridotite: the effects of talc-alteration on strontium and boron isotopes  
609 in abyssal peridotites from Hole 1268a, ODP Leg 209. *Geochimica et Cosmochimica*  
610 *Acta*, 126, 30–48.
- 611 Hirose K, Kushiro I. 1993. Partial melting of dry peridotites at high pressures: determination  
612 of compositions of melts segregated from peridotite using aggregates of diamond.  
613 *Earth Planet. Sci. Lett.* 114:477–89.
- 614 Jayananda, M., Martin, H., Peucat, J.-J. and Mahabaleswar, B., 1995. Late Archaean crust-  
615 mantle interactions in the Closepet granite, Southern India: evidence from Sr–Nd  
616 isotopes, major and trace element geochemistry. *Contributions to Mineralogy and*  
617 *Petrology* **119**, 314–29.
- 618 Jochum, K.P., Stoll, B., Herwig, K., et al., 2006. MPI-DING reference glasses for in situ mi-  
619 croanalysis: new reference values for element concentrations and isotope ratios.  
620 *Geochemistry, Geophysics, Geosystems* 7, <http://dx.doi.org/10.1029/2005GC001060>.

- 621 Kabete, J.M., Groves, D.I., McNaughton, N.J., Mruma, A.H., 2012a. A new tectonic and  
622 temporal framework for the Tanzanian Shield: implications for gold metallogeny and  
623 undiscovered endowment. *Ore Geology Reviews* 48, 88–124.
- 624 Kabete, J.M., McNaughton, N.J., Groves, D.I., and Mruma, A.H., 2012b. Reconnaissance  
625 SHRIMP U–Pb zircon geochronology of the Tanzania Craton: Evidence for  
626 Neoproterozoic granitoid–greenstone belts in the Central Tanzania Region and the  
627 Southern East African Orogen. *Precambrian Research* 216– 219, 232– 266.
- 628 Kamber, B.S., Ewart, A., Collerson, K.D., Bruce, M.C., McDonald, G.D., 2002. Fluid-mobile  
629 trace element constraints on the role of slab melting and implications for Archean  
630 crustal growth models. *Contributions to Mineralogy and Petrology* 144, 38–56
- 631 Kay, R.W., 1978. Aleutian magnesian andesites: melts from subducted Pacific Ocean crust.  
632 *Journal of Volcanology and Geothermal Research* 4, 117–132.
- 633 Kelemen, P.B., K. Hanghøj, and A.R. Greene 2003. One view of the geochemistry of  
634 subduction-related magmatic arcs with an emphasis on primitive andesite and lower  
635 crust, in *The Crust*, (R.L. Rudnick, ed.), Vol. 3, *Treatise on Geochemistry*, (H.D.  
636 Holland and K.K. Turekian, eds.), Elsevier-Pergamon, Oxford, 593-659,
- 637 Kogiso T., Hirschmann M.M., Petermann M., 2004. High-pressure partial melting of mafic  
638 lithologies in the mantle. *Journal of Petrology* 45, 2407-2422.
- 639 Kwelwa, S., 2017. Geological controls on gold mineralization in the Kukuluma Terrain,  
640 Geita Greenstone Belt, NW Tanzania. PhD Thesis, James Cook University,  
641 Townsville, 205pp.

- 642 Kwelwa, S., Manya, S., Vos, I.M.A., 2013. Geochemistry and petrogenesis of intrusions of  
643 the Golden Pride gold deposit in the Nzega Greenstone Belt, Tanzania. African  
644 Journal of Earth Sciences, 86, 53-64.
- 645 Large, R.R., Gemmell, J.B., Paulick, H., and Huston, D.L., 2001. The alteration box plot—A  
646 simple approach to understanding the relationship between alteration mineralogy and  
647 lithochemistry associated with volcanic-hosted massive sulfide deposits:  
648 Economic Geology, 96, 957–971.
- 649 Macpherson, C.G., Dreher, S.T., Thirwall, M.F., 2006. Adakites without slab melting: high  
650 pressure processing of basaltic island arc magma, Mindanao, the Philippines. Earth  
651 and Planetary Science Letters 243, 581–593.
- 652 Manikyamba, C., Kerrich, R., Khanna, T.C., Subba Rao, D.V., 2007. Geochemistry of  
653 adakites and rhyolites from the Neoproterozoic Gadwal greenstone belt, Eastern  
654 Dharwar craton India: implications for sources and geodynamic setting. Canadian  
655 Journal of Earth Sciences 44, 1517–1535.
- 656 Manya, S., and Maboko, A. H. M., 2008. Geochemistry of the Neoproterozoic mafic volcanic  
657 rocks of the Geita area, NW Tanzania: Implications for stratigraphical relationships in  
658 the Sukumaland greenstone belt. Journal of African Earth Sciences 52, 152-160.
- 659 Manya, S., and Maboko, M. A. H., 2003. Dating basaltic volcanism in the Neoproterozoic  
660 Sukumaland Greenstone Belt of the Tanzania Craton using the Sm–Nd method:  
661 implications for the geological evolution of the Tanzania Craton. Precambrian  
662 Research 121, 35-45.

- 663 Many, S., Maboko, M.A.H., 2008. Geochemistry of the Neoproterozoic mafic volcanic rocks  
664 of the Geita area, NW Tanzania: implications for stratigraphical relationships in the  
665 Sukumaland Greenstone belt. *J. Afr. Earth Sci.* 52, 152–160.
- 666 Many, S., Maboko, M.A.H., Nakamura, E., 2007. Geochemistry of high-Mg andesite and  
667 associated adakitic rocks in the Musoma-Mara greenstone belt, northern Tanzania:  
668 possible evidence for Neoproterozoic ridge subduction??. *Precambrian Research* 159,  
669 241–259.
- 670 Many, S., Maboko, M.A.H., 2003. Dating basaltic volcanism in the Neoproterozoic Sukumaland  
671 Greenstone Belt of the Tanzania Craton using Sm–Nd method: implications for the  
672 geological evolution of the Tanzania Craton. *Journal of African Earth Sciences* 121,  
673 35–45.
- 674 Martin, H., 1999. The adakitic magmas: modern analogues of Archaean granitoids. *Lithos* 46  
675 (3), 411–429.
- 676 Martin, H., Moyen, J.F., Rapp, R.P., 2010. The sanukitoid series: magmatism at the  
677 Archaean-Proterozoic transition. *Earth and Environmental Science. Transactions of*  
678 *the Royal Society of Edinburgh* 100 (1–2), 15–33.
- 679 Martin, H., Smithies, R.H., Rapp, R., Moyen, J.F., Champion, D., 2005. An overview of  
680 adakite, tonalite–trondhjemite–granodiorite (TTG), and sanukitoid: relationships and  
681 some implications for crustal evolution. *Lithos* 79, 1–24.
- 682 Mohan, M.R., Piercey, S.J., Kamber, B.S., Sarma, D.S., 2013. Subduction related tectonic  
683 evolution of the Neoproterozoic eastern Dharwar Craton, southern India: new  
684 geochemical and isotopic constraints. *Precambrian Research* 227, 204–226.



- 685 Moyen, J.-F., 2009. High Sr/Y and La/Yb ratios: The meaning of the “adakitic signature”.  
686 Lithos 112, 556–574.
- 687 Moyen, J.-F., 2011. The composite Archaean grey gneisses: petrological significance, and  
688 evidence for a non-unique tectonic setting for Archaean crustal growth. Lithos 123,  
689 21-36.
- 690 Moyen, J.-F., Martin, H., 2012. Forty years of TTG research. Lithos 148, 312–336
- 691 Papoulis D., Tsohis-Katagas, P., and Katagas, C., 2004. Monazite alteration mechanisms and  
692 depletion measurements in kaolins. Applied Clay Science, 24, 271–285.
- 693 Peterson, M. E., A. E. Saal, E. Nakamura, H. Kitagawa, M. D. Kurz, and A. M.  
694 Koleszar (2014), Origin of the “ghost plagioclase” signature in Galapagos melt  
695 inclusions: New evidence from Pb isotopes. Journal of Petrology, 55, 2193–2216.
- 696 Polat, A., Kerrich, R., 2001. Magnesian andesites, Nb-enriched basalt–andesites, and adakites  
697 from late-Archaean 2.7 Ga Wawa greenstone belts, Superior Province, Canada:  
698 implications for late Archean subduction zone petrogenetic processes. Contributions  
699 to Mineralogy and Petrology 141 (1), 36–52.
- 700 Quennell, A.M., McKinley, A.C.M., Aiken, W.G., 1956. Summary of the geology of  
701 Tanganyika: introduction and stratigraphy. Tanganyika Geol. Surv. Mem. 1 (Pt. 1)  
702 264 pp..
- 703 Rapp, R.P., Shimizu, N., Norman, M.D., Applegate, G.S., 1999. Reaction between slab-  
704 derived melts and peridotite in the mantle wedge: experimental constraints at 3.8 GPa.  
705 Chemical Geology 160, 335–356.

- 706 Richards, J. P., and Kerrich, R. 2007. Adakite-like rocks: their diverse origins and  
707 questionable role in metallogensis. *Economic Geology* 102, 537–576.
- 708 Rollinson, H., 1997. Eclogite xenoliths in west African kimberlites as residues from Archean  
709 granitoid crust formation. *Nature* 389, 173–176.
- 710 Romick, J.D., Kay, S.M., Kay, R.M., 1992. The influence of amphibole fractionation on the  
711 evolution of calc-alkaline andesite and dacite tephra from the central Aleutians,  
712 Alaska. *Contributions to Mineralogy and Petrology* 112, 101–118.
- 713 Rooney, T.O., Franceschi, P., Hall, C.M., 2011. Water-saturated magmas in the Panama  
714 Canal region: a precursor to adakite-like magma generation? *Contributions to*  
715 *Mineralogy and Petrology* 161, 373-388.
- 716 Rudnick RL, Gao S. 2003. Composition of the continental crust. See Holland & Turekian  
717 2003, pp. 1–64
- 718 Rudnick, R.L., 1995. Making continental crust. *Nature* 378, 573–578.
- 719 Ryerson F. J. and Watson E. B. (1987) Rutile saturation in magmas: Implications for Ti–Nb–  
720 Ta depletion in island-arc basalts. *Earth and Planetary Science Letters* 86, 225–239.
- 721 Sanislav, I. V., Brayshaw, M., Kolling, S. L., Dirks, P. H. G. M., Cook, Y. A., Blenkinsop,  
722 T., 2016. The structural history and mineralization controls on the world-class Geita  
723 Hill gold deposit, Geita Greenstone Belt, Tanzania. *Mineralium Deposita* – in press.
- 724 Sanislav, I. V., Wormald, R. J., Dirks, P. H. G. M., Blenkinsop, T. G., Salamba, L., Joseph,  
725 D., 2014. Zircon U-Pb ages and Lu-Hf isotope systematics from late-tectonic granites,  
726 Geita greenstone belt: implications for crustal growth of the Tanzania craton.  
727 *Precambrian research* 242, 187-204.

- 728 Sanislav, I.V., Kolling, S.L., Brayshaw, M., Cook, Y.A., Dirks, P.H.G.M., Blenkinsop, T.G.,  
729 Mturi, M.I., Ruhega, R., 2015. The geology of the giant Nyankanga gold deposit,  
730 Geita Greenstone Belt, Tanzania. *Ore Geology Reviews* 69, 1-16.
- 731 Shirey, S. B., Hanson, G. N. 1984. Mantle derived Archaean monzodiorites and  
732 trachyandesites. *Nature* 310, 222-4.
- 733 Shirey, S.B., Hanson, G.N., 1984. Mantle derived Archaean monzodiorites and  
734 trachyandesites. *Nature* 310, 222- 224.
- 735 Spandler, C., Pettke, T., Rubatto, D., 2011. Internal and external fluid sources for eclogite-  
736 facies veins in the Monviso meta-ophiolite, Western Alps: Implications for fluid flow  
737 in subduction zones. *Journal of Petrology*, 52, 1207-1236.
- 738 Spandler, C., Yaxley, G., Green, D. H. and Rosenthal, A., 2008. Phase relations and melting  
739 of anhydrous K-bearing eclogite from 1200 to 1600°C and 3 to 5 GPa. *Journal of*  
740 *Petrology* 49, 771-795.
- 741 Stalder, R., Foley, S.F., Brey, G.P. and Horn, I. 1998. Mineral aqueous fluid partitioning of  
742 trace elements at 900-1200 degrees C and 3.0-5.7 GPa: New experimental data for  
743 garnet, clinopyroxene, and rutile, and implications for mantle  
744 metasomatism. *Geochimica et Cosmochimica Acta* 62, 1781-1801.
- 745 Stern, R. A. Hanson, G. N. and Shirey S. B.. 1989. Petrogenesis of mantle-derived, LILE-  
746 enriched Archaean monzodiorites and trachyandesites (sanukitoids) in southwestern  
747 Superior Province. *Canadian Journal of Earth Sciences*, 26, 168- 171.
- 748 Stockley, G.M., 1936. Geology of the south and south-western region of Musoma District.  
749 Tanganyika Geol. Surv. Short Pap., 13.

- 750 Sun, S. -S., McDonough, W. F., 1989. Chemical and isotopic systematics of oceanic basalts:  
751 implications for mantle composition and processes. In: Saunders, A.D., Norry, M.J.  
752 (Eds.), *Magmatism in the Ocean Basins*. Geol. Soc. London, London, pp. 313–345.
- 753 Sun, Shen-SU and Nesbitt, R.W., 1978. Petrogenesis of Archaean ultrabasic and basic  
754 volcanics: evidence from the rare earth elements. *Contributions to Mineralogy and*  
755 *Petrology* 65, 301-325.
- 756 Tatsumi Y, Ishizaka K. 1981. Existence of andesitic primary magma: An example from  
757 Southwest Japan. *Earth and Planet Science Letters* 53, 124-130.
- 758 Tatsumi Y. 2006 High-Mg Andesites in the Setouchi Volcanic Belt, Southwestern Japan:  
759 Analogy to Archean Magmatism and Continental Crust Formation? *Annu Rev Earth*  
760 *Planet Sci*, 34, 467—499.
- 761 Tatsumi, Y., 2008. Making continental crust: the sanukitoid connection. *Chinese Science*  
762 *Bulletin* 53 (11), 1620–1633.
- 763 Taylor S. R. and McLennan S. M. 1995 *The Geochemical Evolution of the Continental Crust*  
764 *Reviews of Geophysics* 22-2, 241-265
- 765 Thirlwall M. F., Smith T. E., Graham A. M., Theodorou N., HollingsbP., Davidson J. P., and  
766 Arculus R. J. (1994) High field strength element anomalies in arc lavas: source or  
767 process? *Journal of Petrology* 35, 819–838.
- 768 Thorkelson, D.J. and Breitsprecher, K., 2005. Partial melting of slab window margins:  
769 genesis of adakitic and non-adakitic magmas. *Lithos*, 79, 25-41.
- 770 Tiepolo, M., Oberti, R., Zanetti, A., Vannucci, R., Foley, S., 2007. Trace-element partitioning  
771 between amphibole and silicate melt. In: Hawthorne, F.C., Oberti, R., Ventura, G.D.,

- 772 Mottana, A. (Eds.), *Amphiboles: Crystal Chemistry, Occurrence, and Health Issues:*  
773 *Mineralogical Society of America and Geochemical Society, Reviews in Mineralogy*  
774 *and Geochemistry*, 67, pp. 417–452.
- 775 Tulloch, A.J., Kimbrough, D.L., 2003. Paired plutonic belts in convergent margins and the  
776 development of high Sr/Y magmatism: Peninsular Ranges batholith of Baja-  
777 California and Median batholith of New Zealand. *Geological Society of America*  
778 *Special Paper* 374, 1–21.
- 779 van Achterbergh E., Ryan C.G., Jackson S.E., and Griffin, W.L., 2001. Data reduction  
780 software for LA-ICP-MS. In: Sylvester P (ed) *Laser-ablation-ICPMS in the earth*  
781 *sciences: principles and applications*. Mineralogical Association of Canada, Short  
782 *Course* 29, 239–243.
- 783 van Westrenen, W., Blundy, J., Wood, B., 1999. Crystal-chemical controls on trace element  
784 partitioning between garnet and anhydrous silicate melt. *American Mineralogist* 84,  
785 838–847.
- 786 Vlaar, N.J., van Keken, P.E., and van den Berg, A.P., 1994, Cooling of the Earth in the  
787 Archaean: *Earth and Planetary Science Letters*, v. 121, p. 1–18.
- 788 Wang, Q., McDermott, F., Xu, J.F., Bellon, H., Zhu, Y. T., 2005. Cenozoic K-rich adakitic  
789 volcanic rocks in the Hohxil area, northern Tibet: lower-crustal melting in an  
790 intracontinental setting. *Geology* 33, 465–468.
- 791 Wood, D.A., Gibson, I.L. and Thompson, R.N., 1976. Elemental mobility during zeolite  
792 facies metamorphism of the Tertiary basalts of eastern Iceland. *Contributions to*  
793 *Mineralogy and Petrology* 55, 241-254.

794 Woodhead J., Eggins S., and Gamble J. (1993) High field strength and transition element  
795 systematics in island arc and back-arc basin basalts: Evidence for multi-phase  
796 extraction and a depleted mantle wedge. *Earth Planet. Sci. Lett.* **114**, 491–504.

797 Zegers, T.E., van Keken, P.E., 2001. Middle Archean continent formation by crustal  
798 delamination. *Geology* 29, 1083–1086.

799

800

801

ACCEPTED MANUSCRIPT

802 **Figure captions**

803 **Figure 1**

804 Simplified geological map of northern Tanzania (a) and the geological map of Geita  
805 Greenstone Belt (b). SGB – Sukumalanad Greenstone Belt; NZ – Nzega Greenstone Belt; SM  
806 – Shynianga-Malita Greenstone Belt; IS – Iramba-Sekenke Greenstone Belt; KF –  
807 Kilimafedha Greenstone Belt; MM – Musoma-Mara Greenstone Belt. Inset map of Africa  
808 showing the location of Archean blocks.

809 **Figure 2**

810 Geological map of the eastern part of the Geita Greenstone Belt showing the location of the  
811 Kukuluma Intrusive Complex.

812 **Figure 3**

813 Photomicrographs showing the three main rock types found in the KIC. a and b) Medium  
814 grained diorite; the mineralogy is dominated by amphibole (mostly actinolite) and plagioclase  
815 with minor quartz. c and d) Medium grained monzonite; the mineralogy is dominated  
816 plagioclase, k-feldspar, biotite and amphibole with minor quartz. The diorite and monzonite  
817 have been deformed and metamorphosed to greenschist facies. As a result amphiboles and  
818 pyroxenes have been partly replaced by actinolite. Note that the feldspars in both rock types  
819 are not altered to sericite and appear fresh under microscope suggesting that the samples have  
820 not been significantly affected by hydrothermal alteration. e and f ) Photographs of a  
821 porphyritic granodiorite dyke. Note that the feldspars from the granodiorite have been partly  
822 replaced by sericite but appear mostly fresh under microscope. Small amounts of carbonate  
823 and chlorite, disseminated or as microveins are present in all samples.

824



825 **Figure 4**

826 Series of diagrams showing that although the rocks of the KIC have been hydrated and  
827 carbonated, as indicated by the petrography and LOI values, their major and trace element  
828 composition was very little disturbed. In the alteration boxplot of Large et al. (2001) all  
829 samples plot in the field of least altered rocks (a). Diagrams b and c show that there is no  
830 correlation between the concentration of two of the most mobile major elements, Na<sub>2</sub>O and  
831 K<sub>2</sub>O, and the LOI values. The same pattern is observed in d and e where the concentration of  
832 two of the most mobile trace elements, Rb and Sr, are plotted against the LOI values  
833 suggesting that most likely the concentration of these elements is close to their initial values.  
834 The mobility of REE and HFSE was tested by plotting the values of La (f) and Nb (g) against  
835 Zr, a highly immobile element. The good correlations suggest that these elements were most  
836 likely immobile during post-magmatic alteration and metamorphism.

837 **Figure 5**

838 Major elements variation diagrams for the KIC. The grey area shows the field of sanukitoids  
839 from Martin et al., (2010). The field of LSA (continuous line in Figure 5b) is from Castillo  
840 (2012) and the field of basaltic experimental melts is from Rollison (1997) and Martin et al.,  
841 (2005).

842 **Figure 6**

843 Chondrite normalized REE diagrams (a, c and e) and primitive mantle normalized trace  
844 element diagrams (b, d and f) for the KIC rocks. Also shown is the average of LSA, HSA,  
845 sanukitoids and Closepet-type granite from Martin et al., (2005).

846 **Figure 7**

847 Sr/Y vs Y (a) and La/Yb<sub>n</sub> vs Yb<sub>n</sub> (b) diagrams for the KIC samples. The field of LSA (light  
848 grey) and HSA (darker grey) in (a) is from Castillo (2012) and the field of sanukitoids  
849 (dashed line) is from Martin et al., (2005). The field of adakites in (b) is from Moyen and  
850 Martin (2012). The diagrams in (c) and (d) show that the samples that have high Sr/Y (c) and  
851 La/Yb<sub>n</sub> ratios (d) also have high Dy/Yb<sub>n</sub> ratio indicative of high pressure melting. The large  
852 square (diorite suite) and the large circle (monzonite suite) show the samples with the highest  
853 Mg# which also have the Sr/Y, La/Yb<sub>n</sub> and Dy/Yb<sub>n</sub> ratios. The line with arrow in (d) shows  
854 that the interaction of eclogitic melts with the mantle peridotite leads to a decrease in the  
855 La/Yb and Dy/Yb ratios in the melt (Kelemen et al., 2003).

856 **Figure 8**

857 Diagram (a) showing that at similar CaO values the monzonite suite has higher Na<sub>2</sub>O which  
858 may reflect clinopyroxene in the source and melting at higher pressure. The lack of  
859 correlation (b) between the MgO and the Sr/Sr\* suggest that the Sr anomaly is not the result  
860 of plagioclase fractionation. (c) shows that Zr and Hf are fractionated from each other in the  
861 monzonite suite which we attribute to residual rutile. The effect of residual rutile is shown in  
862 (d) where the positive correlation between Nb/La and Zr/Sm ratios is indicative of residual  
863 rutile (Münker et al., 2004). The dashed lines in (c) and (d) shows the chondritic ratios for the  
864 respective elements while the arrows in (d) show the effect of residual rutile (positive  
865 correlation) vs the effect of residual high-Mg amphibole (negative correlation).

866 **Figure 9**

867 Diagrams showing the compositional differences between LSA and HSA on K vs Rb (a), Sr  
868 vs CaO+Na<sub>2</sub>O (b) and Cr/Ni vs TiO<sub>2</sub> (c) compiled by Martin et al., (2005). In (a) the  
869 continuous line shows the average K/Rb ratio in MORB (Sun and McDonough, 1989) while  
870 the arrows show the effect of metasomatism, which increases the ratio and the effect of

871 partial melting, which decreases the ratio. In all three diagrams the KIC samples resemble  
872 more the HSA than the LSA and mostly overlap the field of experimental basaltic melts. The  
873 diagram in (d) show that there is no correlation between the Cr/Ni ratio and the Mg#  
874 indicating that the Cr/Ni ratio in the KIC samples is a source characteristic rather than the  
875 result of fractionation.

876 **Figure 10**

877 Diagram showing the variation of the Sr/Y ratio with MgO in modern arcs, Archean adakites  
878 and experimental melts from Chiaradia (2015). Chiaradia (2015) showed that in the modern  
879 arcs the Sr/Y ratio is a function of crustal thickness and the gradual increase of the Sr/Y ratio  
880 with increased crustal thickness also correlates with decreasing MgO suggesting that the Sr/Y  
881 ratio in modern arcs better reflects intracrustal processes than source characteristics. The  
882 sudden increase in Sr/Y ratios at low MgO in Archean adakites is similar to the data obtained  
883 for experimental basaltic melts and is consistent with partial melting of the lower mafic crust  
884 in the Archean. The KIC samples have Sr/Y and MgO values similar to the experimental  
885 basaltic melts and the Archean adakites suggesting lower mafic crust melting. The diagram in  
886 (b) shows that the diorite and the granodiorite suite have near MORB/chondritic Zr/Hf and  
887 Th/U ratios while the monzonite suite has Zr/Hf ratios similar to the mafic end member (mlc)  
888 of the lower crust (Hacker et al, 2015) and the Th/U ratio varies between the mafic end  
889 member of the lower crust and the lower continental crust (lcc) values of Rudnick and Gao  
890 (2003). However, the Th/U ratios in all samples are near chondritic suggesting that Th and U  
891 were not fractionated from each other as required by a subduction environment.

892

893

Element	LSA	HSA	Sanukitoid	Closepet	Monzonite suite	Diorite suite	Granodiorite	KIC (average)
SiO <sub>2</sub> (%)	56.25	64.80	58.76	56.39	56.41	58.61	62.50	57.51
TiO <sub>2</sub> (%)	1.49	0.56	0.74	1.20	0.49	0.51	0.55	0.50
Al <sub>2</sub> O <sub>3</sub> (%)	15.69	16.64	15.80	15.79	15.70	16.09	15.69	15.90
FeO (%)	5.82	4.27	5.28	6.60	5.71	6.39	4.89	6.05
MnO (%)	0.09	0.08	0.09	0.13	0.07	0.08	0.08	0.07
MgO (%)	5.15	2.18	3.90	3.38	3.54	2.90	1.89	3.22
CaO (%)	7.69	4.63	5.57	5.45	4.99	4.58	3.71	4.79
Na <sub>2</sub> O (%)	4.11	4.19	4.42	3.94	5.61	4.20	3.37	4.90
K <sub>2</sub> O (%)	2.37	1.97	2.78	3.17	2.59	2.16	3.67	2.38
P <sub>2</sub> O <sub>5</sub> (%)	0.66	0.20	0.39	0.72	0.50	0.22	0.16	0.36
K <sub>2</sub> O/Na <sub>2</sub> O	0.58	0.47	0.63	0.80	0.49	0.51	1.10	0.50
CaO+Na <sub>2</sub> O	11.80	8.82	9.99	9.39	10.59	8.78	7.08	9.69
FeO+MgO+MnO+TiO <sub>2</sub>	12.55	7.09	10.01	11.31	9.81	9.88	7.42	9.85
Y (ppm)	13.00	10.00	18.00	37.00	17.24	9.794	16.41	13.52
Yb (ppm)	0.93	0.88	1.32	2.05	1.18	0.85	1.57	1.02
Sr (ppm)	2051.00	565.00	1170.00	978.00	1128.38	834.34	331.96	981.36
Cr (ppm)	157.00	41.00	128.00	50.00	86.91	75.10	21.24	81.00
Ni (ppm)	103.00	20.00	72.00	38.00	46.65	53.00	13.43	49.83
Sr/Y	162.21	55.65	63.98	26.43	71.39	85.19	20.25	78.29
La/Yb	44.19	21.82	45.38	44.34	82.76	26.68	15.20	54.72
Mg#	0.61	0.48	0.57	0.48	0.53	0.46	0.41	0.49

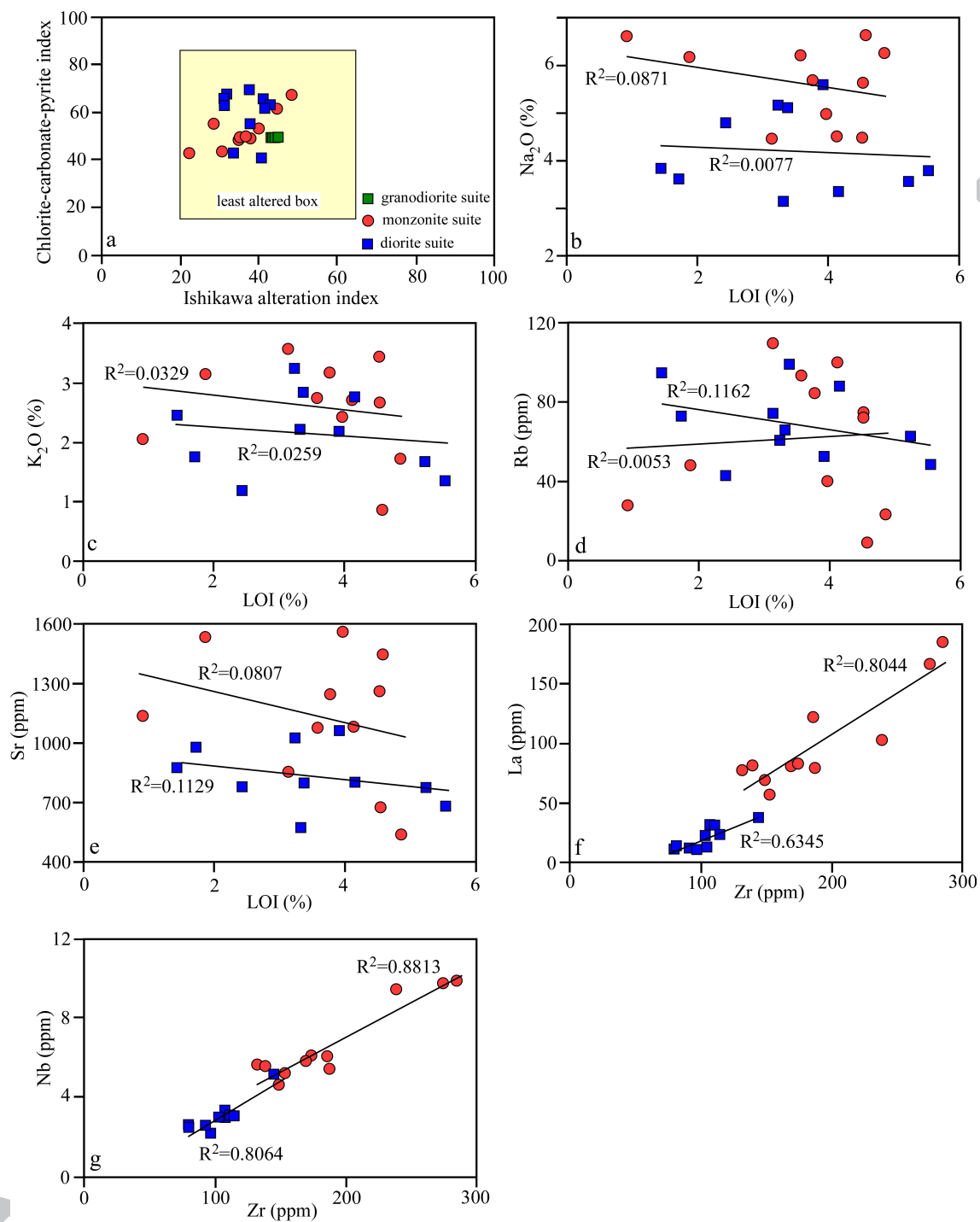
894

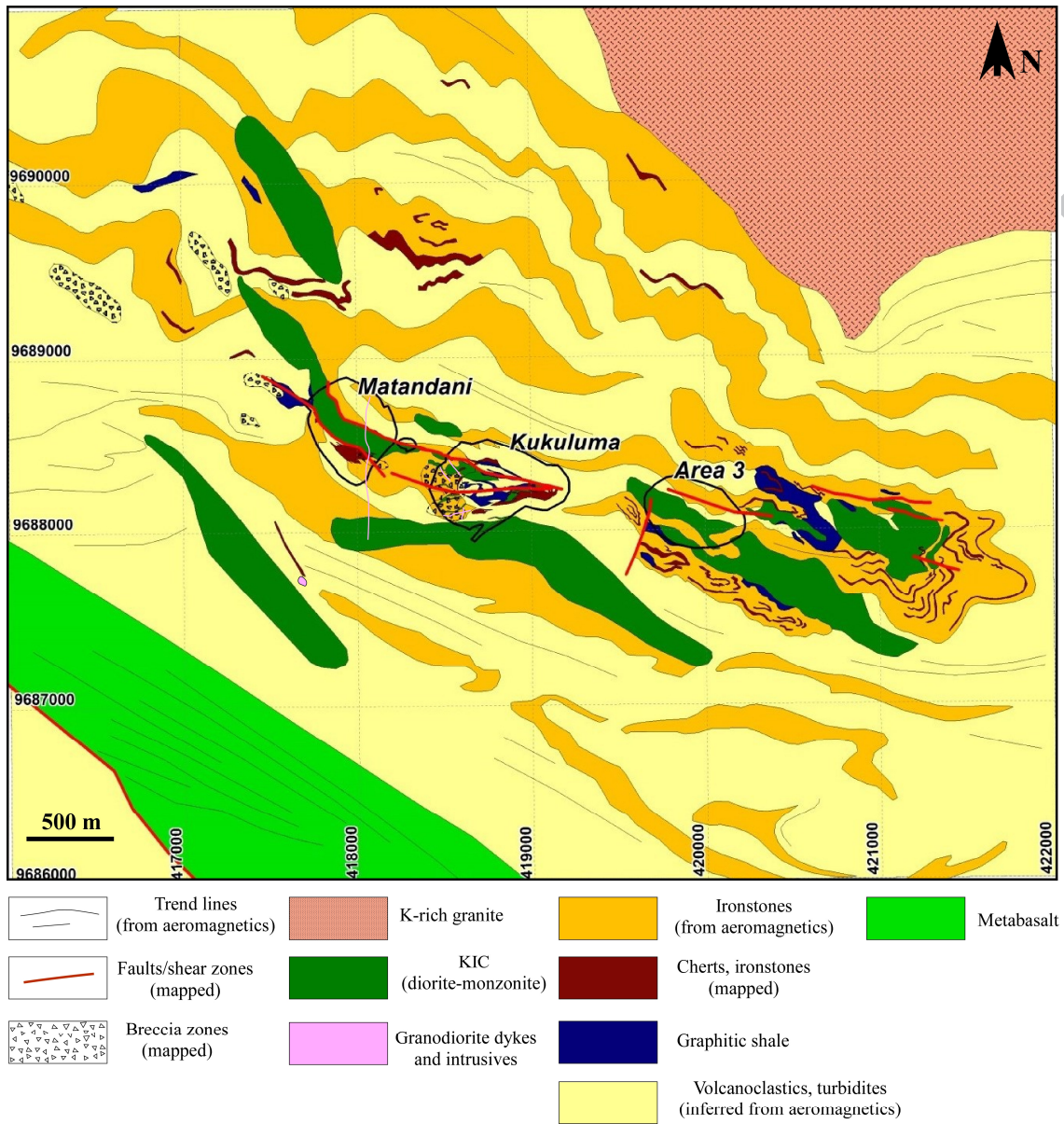
895 **Table 1.** Table showing the average composition of the adakites, sanukitoids and Closepet-  
896 type granite (Martin et al., 2005) and the average composition of the Kukuluma Intrusive  
897 Complex rocks.

898

899

900



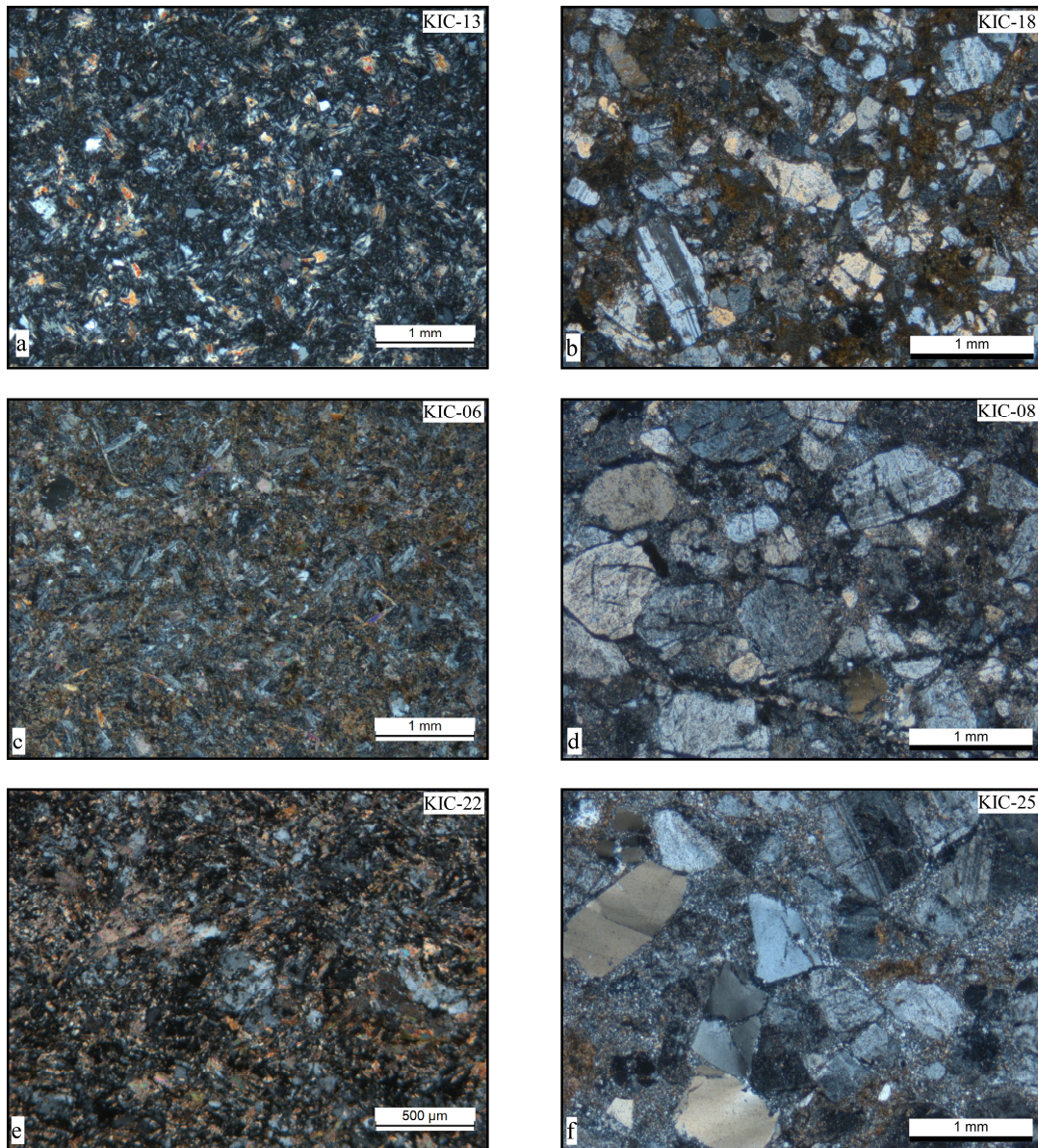


902

Figure 2

903



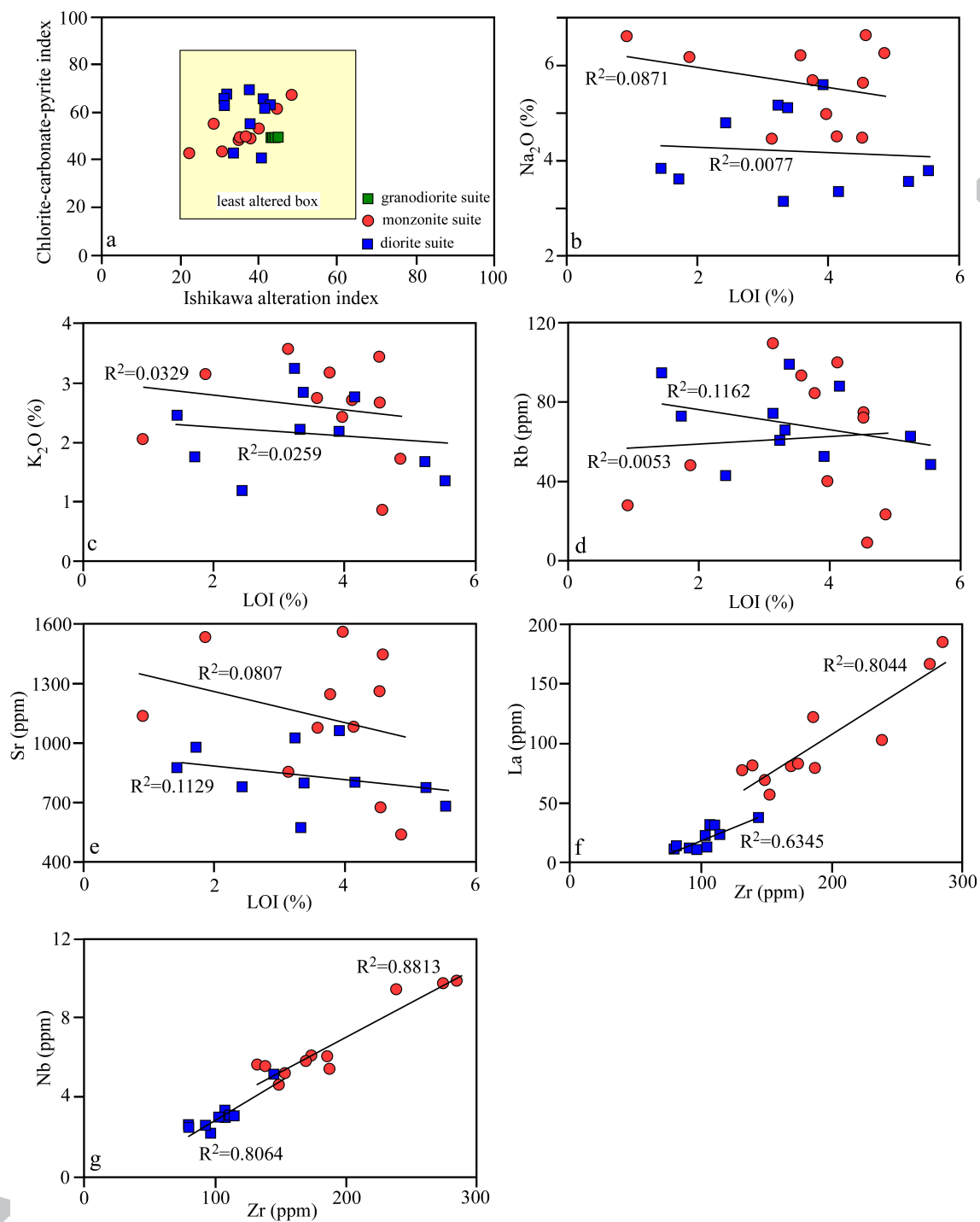


904

Figure 3

905





906

Figure 4

907

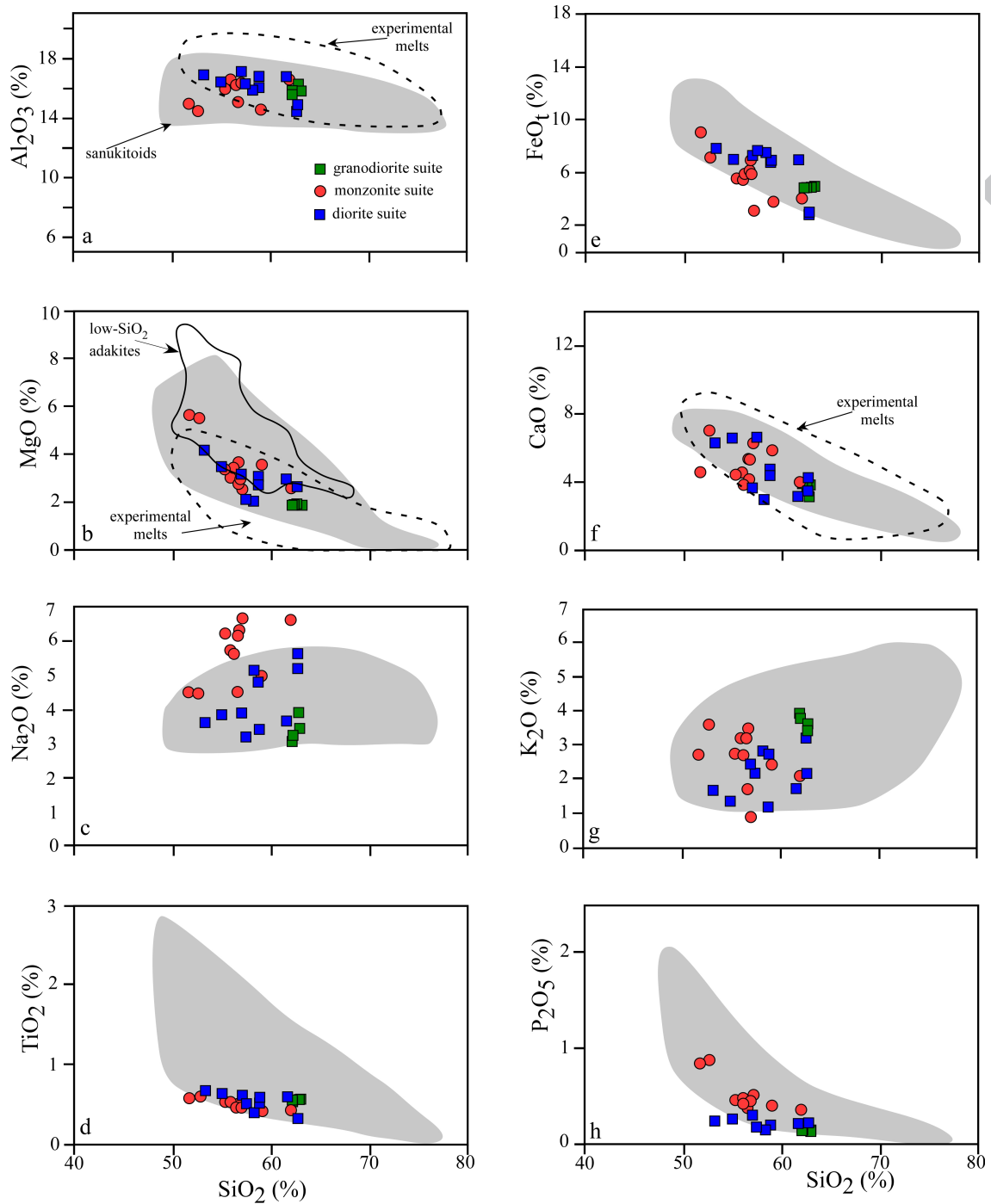
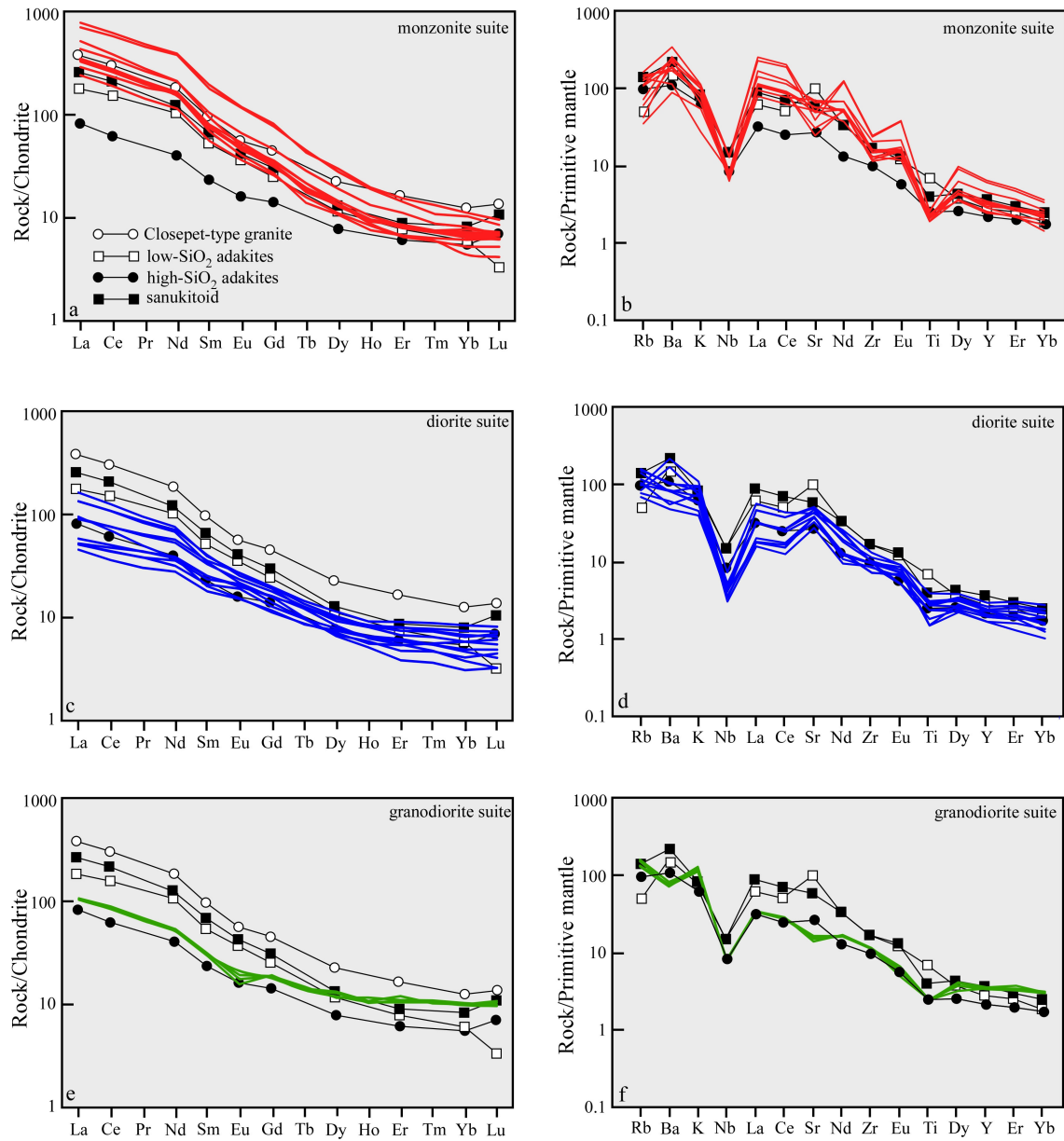


Figure 5

908

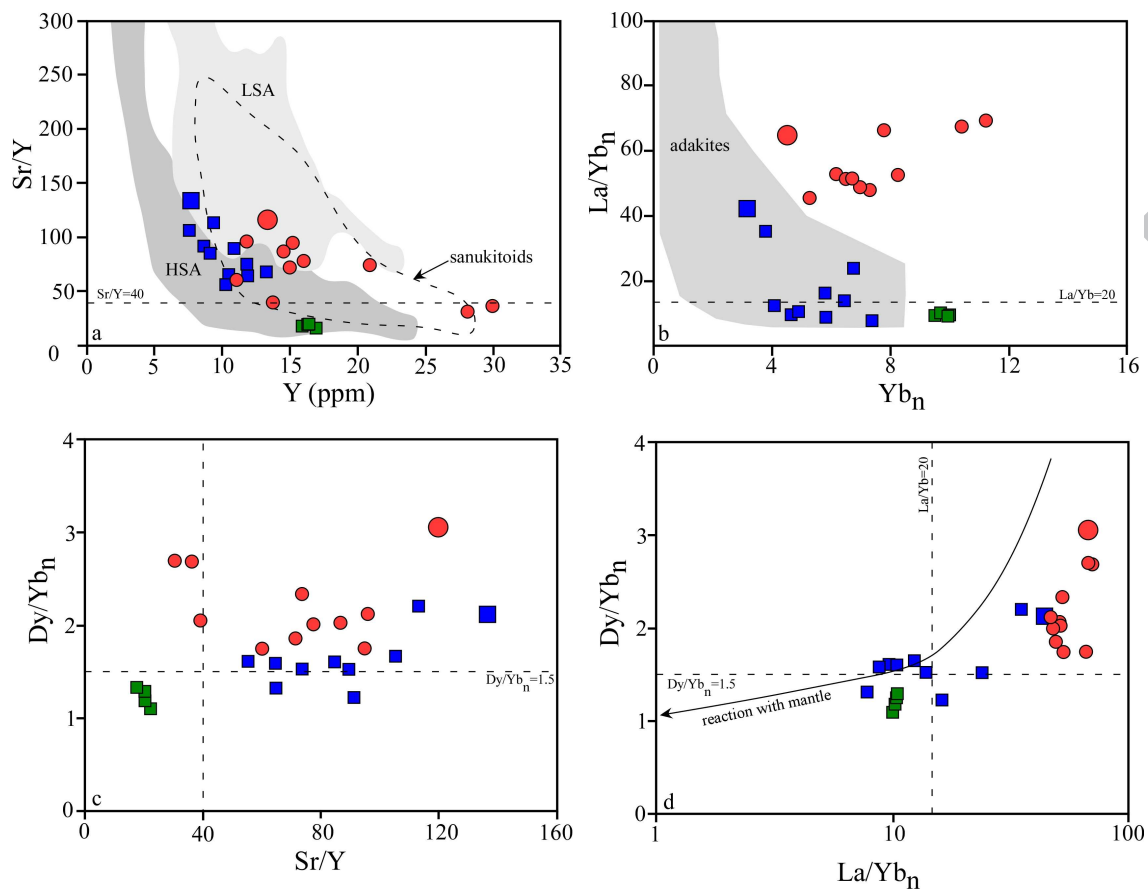
909



910

Figure 6

911

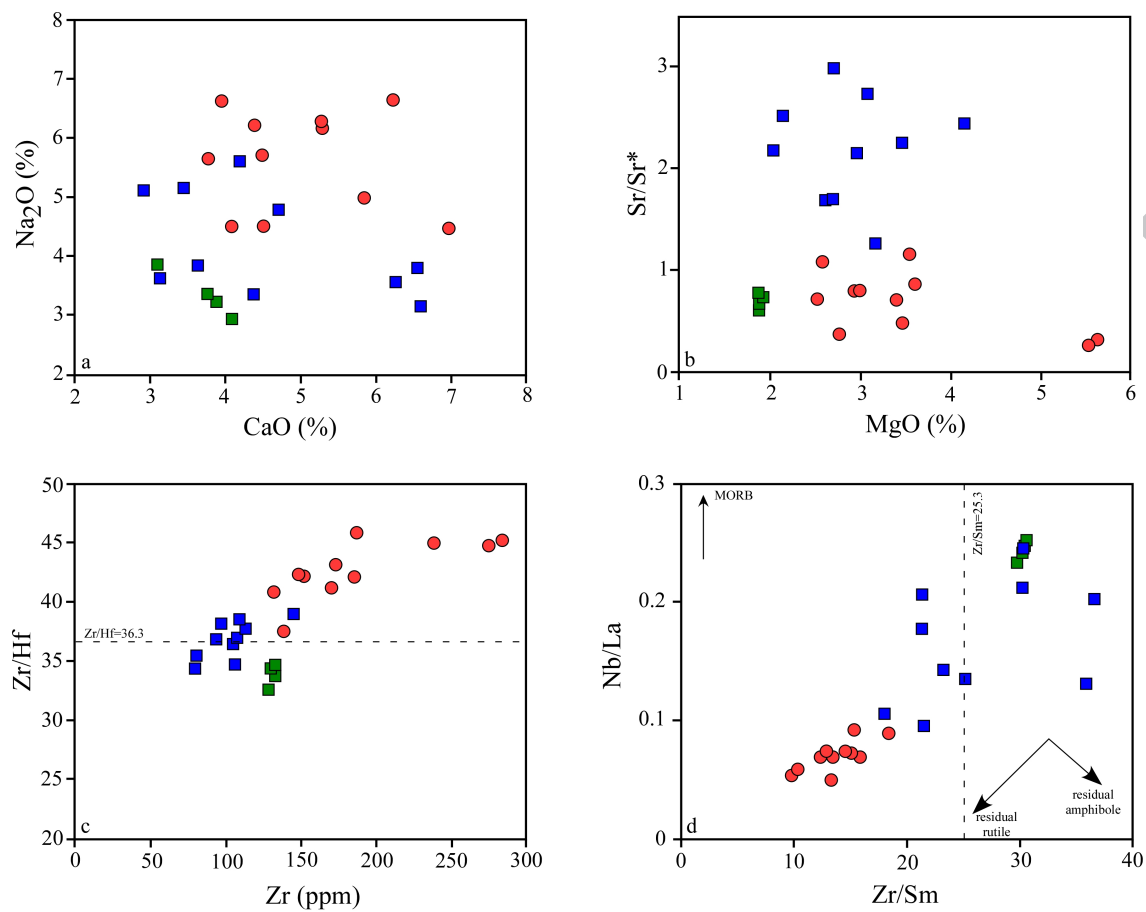


912

Figure 7

913

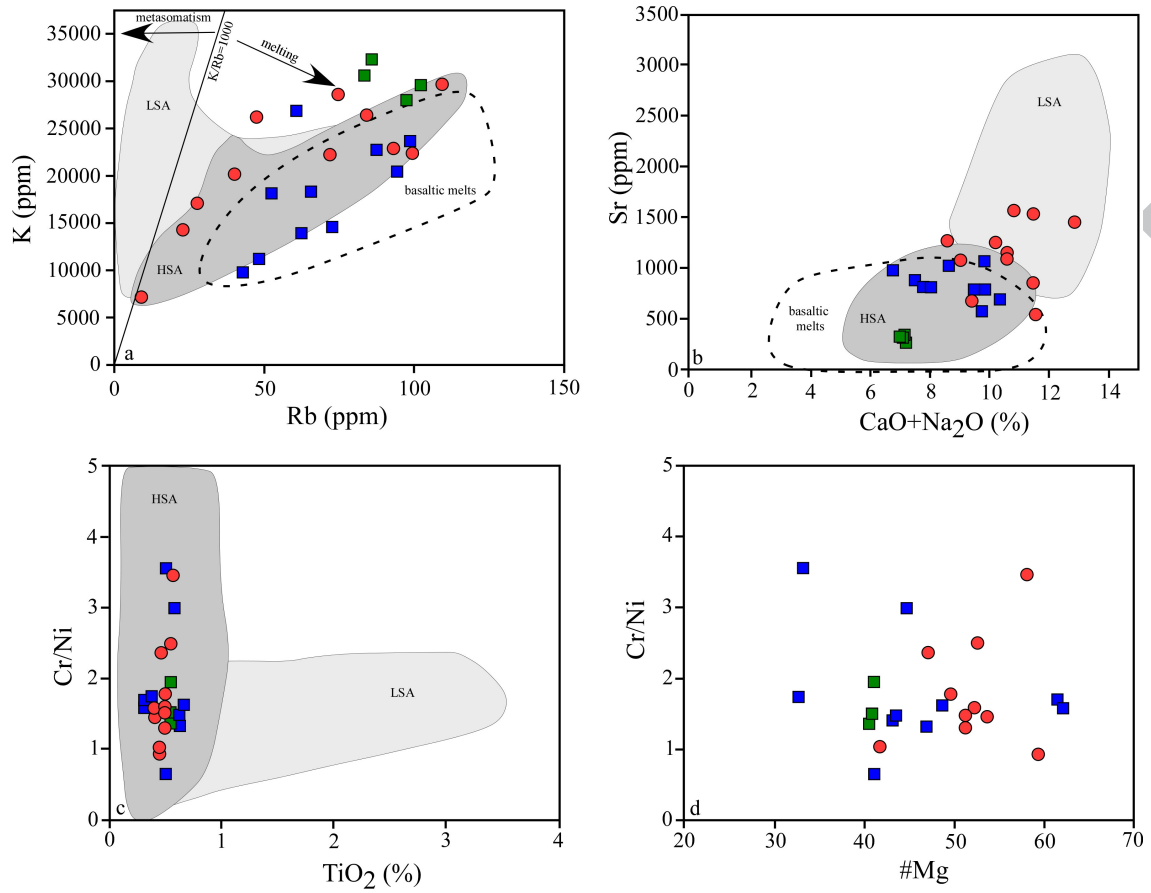
ACCEPTED



914

Figure 8

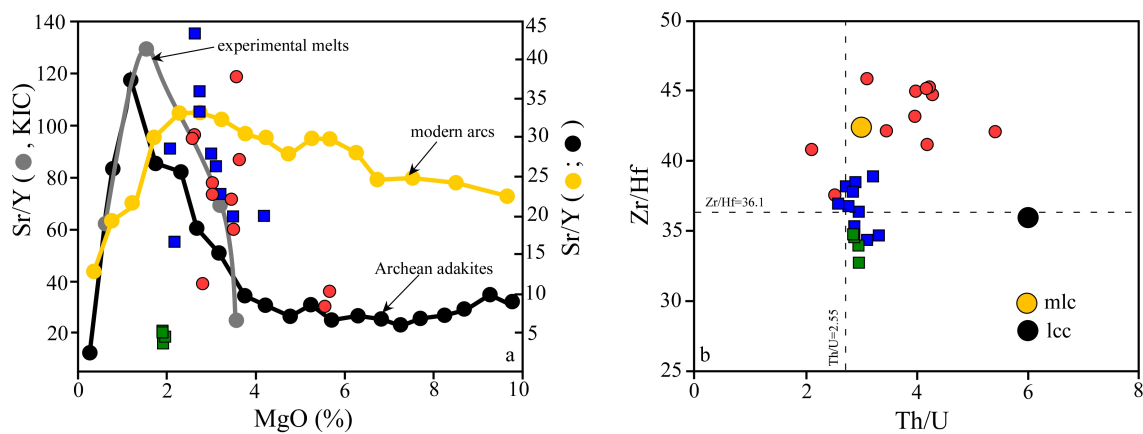
915



916

Figure 9

917



918

Figure 10

919



920 **Highlights**

- 921       • The KIC is a syn-tectonic Neoproterozoic igneous complex with intermediate composition
- 922       • The KIC has high Sr/Y and La/Yb ratios indicative of a melting in the garnet stability field
- 923       • The KIC formed by partial melting of thickened mafic/ultramafic lower crust
- 924       • The KIC is related to the removal of the eclogitised root of an oceanic plateau

925

ACCEPTED MANUSCRIPT